J. Fluid Mech. (1991), *vol.* 228, *pp.* 53–86
Printed in Great Britain

The velocity and vorticity vector fields of a turbulent boundary layer. Part 2. Statistical properties

By JEAN-LOUIS BALINT, JAMES M. WALLACE AND PETAR VUKOSLAVČEVIĆ†
Department of Mechanical Engineering, The University of Maryland, College Park, MD 20742, USA

(Received 12 January 1990 and in revised form 14 December 1990)

Many of the statistical properties of both the velocity and the vorticity fields of a nominally zero-pressure-gradient turbulent boundary layer at $R_\delta = 27650$ ($R_\theta = 2685$) have been simultaneously measured. The measurements were made with a small nine-sensor hot-wire probe which can resolve the turbulence to within about six Kolmogorov microscales just above the sublayer. The statistical properties of the velocity vector field compare very well with other laboratory measurements and with direct numerical simulations when Reynolds-number dependence is taken into account. The statistical properties of the vorticity field are also in generally good agreement with the few other measurements and with the direct numerical simulations available for comparison. Near the wall, r.m.s. measurements show that the fluctuating spanwise vorticity is the dominant component, but in the outer part of the boundary layer all the component r.m.s. values are nearly equal. R.m.s. measurements of the nine individual velocity gradients show that the gradients normal to the wall of all three velocity components are the largest, with peaks occurring near the wall as expected. Gradients in the streamwise direction are everywhere small. One-dimensional spectra of the vorticity components show the expected shift of the maximum energy to higher wavenumbers compared to spectra of the velocity components at the same location in the flow. The budget of the transport equation for total enstrophy indicates that the viscous dissipation rate is primarily balanced by the viscous diffusion rate in the buffer layer and by the rotation and stretching rate in the logarithmic layer.

1. Introduction

In Part 1 of this paper (Vukoslavčević, Wallace & Balint 1991), a miniature probe with nine hot-wire sensors was described. It has been used to simultaneously measure the velocity and vorticity vectors in and above the buffer layer in a turbulent boundary layer with spatial resolution, at worst, of about six Kolmogorov microscales at a moderate Reynolds number. Such data have not been otherwise obtained experimentally to date. We briefly reviewed in Part 1 other hot-wire methods previously used to measure some vorticity components and referred to direct numerical computer simulations (DNS) which have been used to determine all three components of the velocity and vorticity vectors. Here in Part 2 we will present

† On leave from the Veljko Vlahović University, 81000 Titograd, Yugoslavia.

many of the statistical properties of the velocity and vorticity vector components measured simultaneously in a turbulent boundary layer at a Reynolds number of $R_\delta = 27650$, where δ is the boundary-layer thickness. These results will be compared to the few available laboratory measurements and to the DNS results mentioned above. The statistical properties of the velocity vector components will be presented primarily in order to demonstrate further the accuracy of the probe. It should be additionally stressed however, as described in Vukoslavčević & Wallace (1981) and mentioned in Part 1, that our nine-sensor probe is the *only* hot-wire method which is able to account for and incorporate into its operation, to first order, the non-uniformity of the velocity field over the probe sensing area. This is particularly important for instances when the probe encounters large local velocity gradients which cannot be accounted for by other hot-wire probes with fewer than nine sensors. Such occurrences are frequent in highly sheared turbulence such as the wall region of a turbulent boundary layer. These velocity statistics, with two exceptions only, will be compared to results from methods which are also capable of measuring or simulating one or more of the vorticity components. For the turbulent boundary layer, the only other available hot-wire laboratory measurements which included a component of the vorticity vector are those of Klewicki (1989) at the three Reynolds numbers $R_\delta = 10390$, 29520, and 49885. The spanwise vorticity component in his investigation was measured with the probe designed by Foss (1981). In the near-wall region, i.e. the viscous and buffer layers and the lower part of the logarithmic layer, channel flow measurements of the streamwise vorticity component made by Kastrinakis & Eckelmann (1983) are also available for comparison at $R_{\frac{1}{2}d} = 12600$, where $\frac{1}{2}d$ is the channel half-width. The turbulent boundary layer has been numerically simulated by Spalart (1988) for the Reynolds numbers $R_\delta = 6890$ and 14500; the near-wall region can also be compared to the channel flow simulation of Kim, Moin & Moser (1987) at $R_{\frac{1}{2}d} = 3300$. These simulations provide full field velocity and vorticity statistics for all components. In order to compare some of our velocity statistics with a higher-Reynolds-number boundary-layer experiment which has an established place in the literature, we also show the results of Klebanoff (1954) at $R_\delta = 78000$. A recent channel flow investigation by Wei & Willmarth (1989) over the Reynolds number range $R_{\frac{1}{2}d} = 2970$–39582 using a high-resolution laser-Doppler velocimeter has helped to clarify the dependence on Reynolds number of many of the streamwise and normal velocity component statistics. Because the effects of Reynolds number are separated fairly well from the effects of probe resolution for the velocity measurements in this study, these data will also be compared and discussed in order to demonstrate Reynolds-number dependence for all the comparison data sets.

Table 1 lists the various investigations to which our measurements are compared, together with the velocity and vorticity components measured in each investigation, the spatial resolution of the method, and the Reynolds number of each investigation. The Kolmogorov lengthscale η for each of these investigations has been estimated based on our measurement of the dimensionless dissipation rate $\epsilon^+ = \epsilon\nu/u_\tau^4 \approx -0.1$ at $y^+ = 15$, which is found in figure 10. Here $u_\tau = (\tau_w/\rho)^{\frac{1}{2}}$ is the friction velocity, ν is the kinematic viscosity, τ_w is the wall stress and ρ is the fluid density. Our value of ϵ^+ for $R_\delta = 27650$ is in quite good agreement with the simulation result of Mansour, Kim & Moin (1988). There is some evidence that ϵ^+ is dependent on the Reynolds number, but doubling the value of ϵ^+ to -0.2 only increases the ratio of $\Delta l/\eta$ at $y^+ = 15$ from 2.2 to 2.6 for the Wei & Willmarth (1989) investigation for example, where Δl is the resolved length of the measurement. In table 2, the symbols used throughout the

Investigation	Type of flow	R_δ or $R_{\frac{1}{2}d}$	Velocity and vorticity components measured						Spatial resolution or grid size: Viscous length			Ratio to η (at $y^+ = 15$)		
			u	v	w	ω_x	ω_y	ω_z	Δx^+	Δy^+	Δz^+	$\Delta x/\eta$	$\Delta y/\eta$	$\Delta z/\eta$
Present	Boundary layer	27650	×	×	×	.	.	.	10.9	10.9	10.9	6.3	6.3	6.3
			.	.	.	×	×	×	10.9	10.9	10.9	6.3	6.3	6.3
Balint *et al.* (1987)	Boundary layer	21375	×	×	×	.	.	.	8.3	8.3	8.3	5.0	5.0	5.0
			.	.	.	×	×	×	8.3	8.3	8.3	5.0	5.0	5.0
Kastrinakis & Eckelmann (1983)	Channel	12600	×	×	×	.	.	.	.	11.5	11.5	.	6.5	6.5
			.	.	.	×	.	.	.	11.5	11.5	.	6.5	6.5
Kim *et al.* (1987)	Channel	3300	×	×	×	.	.	.	12.0	0.05–4.4	7.0	6.7	0.8	3.9
			.	.	.	×	×	×	12.0	Same	7.0	6.7	0.8	3.9
Klebanoff (1965)	Boundary layer	78000	×	×	×	.	.	.	.	20.3	20.3	.	11.4	11.4
Klewicki (1989)	Boundary layer	29520	×	×	.	.	.	.	.	4.8	4.8	.	2.7	2.7
			.	.	.	.	.	×	.	.	16.2	.	.	9.1
Spalart (1988)	Boundary layer	14500	×	×	×	.	.	.	20.0	0.24–3.30	6.7	11.2	1.2	3.8
			.	.	.	×	×	×	20.0	Same	6.7	11.2	1.2	3.8
Wei & Willmarth (1989)	Channel	22776	×	×	.	.	.	.	3.9	3.9	3.9	2.2	2.2	2.2

TABLE 1. Types of flow, Reynolds numbers and spatial resolution information of comparison data sets

paper for these comparisons data, unless otherwise stated in the captions, are displayed.

2. Experimental facility and instrumentation

This investigation was carried out in a low-speed, open-return wind tunnel which was designed to create a thick turbulent boundary layer in order to obtain good probe spatial resolution for these vorticity measurements. The boundary layer developed on the lower wall of the tunnel over a 8 m fetch downstream of a 5 mm trip wire used to fix transition as verified by smoke streakline flow visualization. The speed range of the free-stream core of the tunnel can be varied over about 1–7 m/s with a free-stream turbulence level of about 0.5% at the lowest speeds. The spanwise variation of the mean velocity in the core is less than 1.5%.

The nine hot-wire sensors of the vorticity probe were heated by constant-temperature anemometry circuits built by AA Lab Systems. The frequency response of the anemometer system for the flow speed studied was flat up to about 4000 Hz, which is much greater than the highest frequency at which there is any significant energy in the flow at the Reynolds number studied here as determined from single-sensor probe spectra. The anemometer output voltages were amplified and digitized with a 12 bit Data Translation simultaneous sample and hold A/D converter

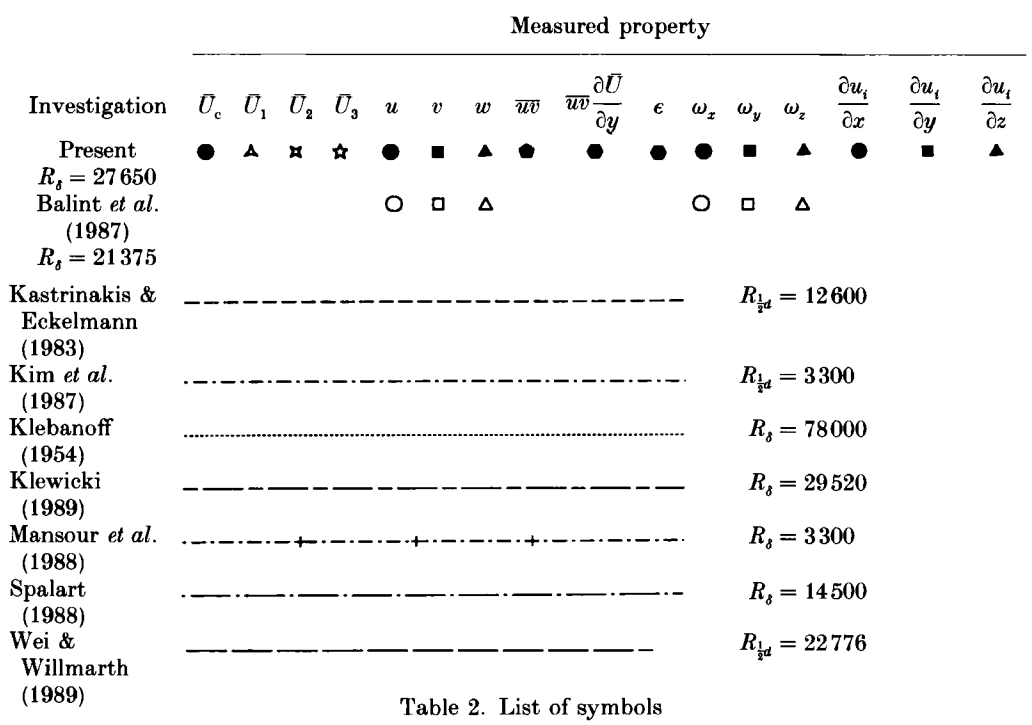

Table 2. List of symbols

operated by a DEC LSI 11/23 microprocessor. The data were sampled at the rate of 1000 Hz, i.e. with a Nyquist frequency of 500 Hz, so that two consecutive sampling periods, when converted to a streamwise length using Taylor's hypothesis, would be of about the same dimension as the 1.2 mm cross-stream dimension over which the cross-stream velocity gradients were determined by finite difference. At each location the data were continuously sampled for 180 s, which was found to be adequately long to obtain stationary higher-order statistics. The data were initially stored on a Winchester hard disk before being transferred to the disk of a Sun 3/260 minicomputer for post-processing.

3. Velocity component statistical properties

3.1. *Mean properties*

In table 3 are listed several of the characteristics of the boundary layer investigated in this study as well as those for the earlier, somewhat lower Reynolds number preliminary study of Balint, Vukoslavčević & Wallace (1987). Here U_∞ is the free-stream velocity in the core of the tunnel, δ is the boundary-layer thickness, θ is the momentum thickness, δ^* is the displacement thickness, $H = \delta^*/\theta$ is the shape factor, and R_δ and R_θ are the Reynolds numbers based on δ and θ respectively. The friction velocity was determined by the Clauser method of choosing a value which causes the data in the logarithmic region to fit best, in a least-squares sense, the logarithmic law using the constants found by Coles (1962).

In the earlier investigation of Balint *et al.* (1987), a probe of the same design was used, but it was slightly larger, i.e. the vertical spacing between arrays 1 and 3 was 1.5 mm and the horizontal spacing was 1.3 mm. It also had somewhat larger

	U_∞ (m/s)	u_τ/U_∞	δ (m)	θ (m)	δ^* (m)	H	R_δ	R_θ
Present	3.51	0.041	0.125	0.0121	0.0156	1.29	27650	2685
Balint *et al.* (1987)	2.39	0.042	0.140	0.0136	0.0175	1.28	21375	2080

TABLE 3. Boundary-layer characteristics

common-prong resistances of about 0.1–0.13 Ω. Moreover, in the earlier experiment, there was a greater percentage of the data near the wall which did not converge to a solution than in the present experiment (9.8% at $y^+ = 14.1$, 8.0% at $y^+ = 20.4$, 6.6% at $y^+ = 30.6$ compared to the values for the present data given in Part 1) which undoubtedly accounts for some of the differences in the results. In fact the problems with the earlier experiment very near the wall motivated us to repeat the experiment with the improved probe for locations within the fully turbulent region ($y/\delta \leqslant 0.4$). We increased the Reynolds number by a factor of almost 1.3 in order to have a higher signal-to-noise ratio for the vorticity measurements with about the same spatial resolution because the new probe size was a little smaller.

Figure 1 shows the mean velocity variation of the boundary layer with the distance from the wall normalized with the friction velocity u_τ and the kinematic viscosity ν. In figure 1(*a*) our present measurements determined at the geometric centre of the three arrays are shown. In figure 1(*b*), the values of the mean velocity measured at each of the three individual arrays of the nine-sensor probe in the present investigation are also shown. The values measured at the centre of the probe and at each array separately show the expected logarithmic form given by Coles (1962):

$$U^+ = 2.44 \ln y^+ + 5.0. \tag{1}$$

The buffer-layer data also agree very well with an empirical fit given by Spalding (1961) except at one location. The mean velocity values measured by all three arrays and at the probe centroid are low when the probe was centred at $y^+ = 18$. These low mean values can be accounted for by a possible vertical positioning error of about 0.1 mm at this location which corresponds to about one viscous length.

3.2. *Moments of velocity fluctuation components*

In figure 2(*a–c*), the r.m.s. values of the three fluctuating velocity components at the centre of the probe, normalized with the outer variables u_τ and δ are compared to the higher-Reynolds-number boundary-layer measurements of Klebanoff (1954) and to the boundary-layer simulation of Spalart (1988), as well as to our earlier values. For $y/\delta \geqslant 0.05$ all four sets of data agree very well. Near the wall Klebanoff's (1954) measurements show larger values for all three components with this scaling.

The same data, normalized with the wall variables ν and u_τ, are plotted in figure 3(*a–c*) against y^+ for the buffer layer and the lower part of the logarithmic layer where they are compared to the results of several other boundary layer and channel flow investigations. Our streamwise component measurements, seen in figure 3(*a*), compare extremely well with those of Wei & Willmarth (1989) made at only a slightly lower Reynolds number. The range between their highest and lowest Reynolds numbers is shown hatched in order to demonstrate Reynolds-number dependence. The values of Kim *et al.* (1987) for the very low Reynolds number $R_{\frac{1}{2}a} = 3300$ reflect this Reynolds-number dependence. Wei & Willmarth (1989) established that the wall

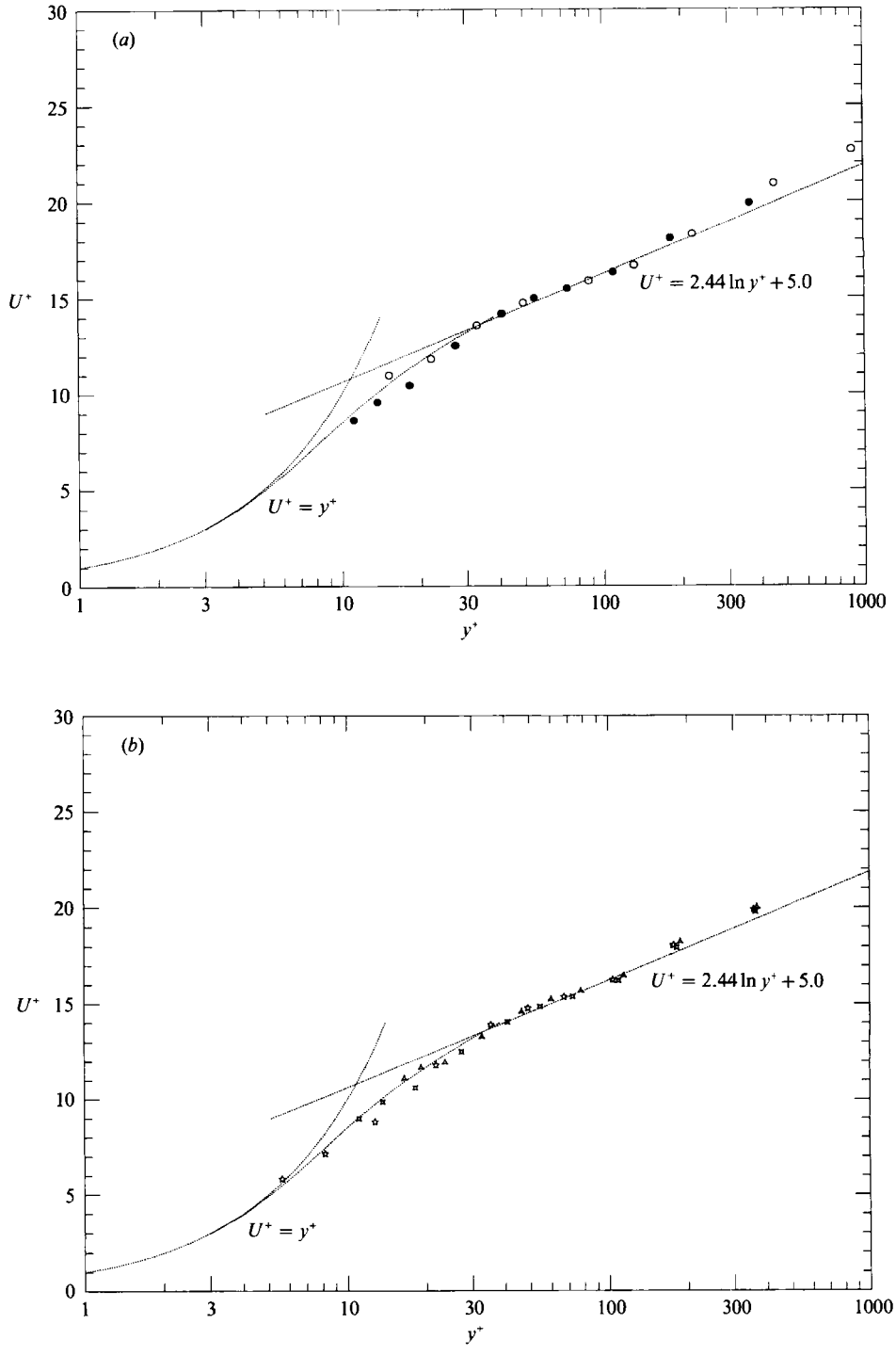

FIGURE 1. (*a*) Mean velocity at the geometric centre of the probe. (*b*) Mean velocity at each of the three arrays of the probe. Symbols given in table 2.

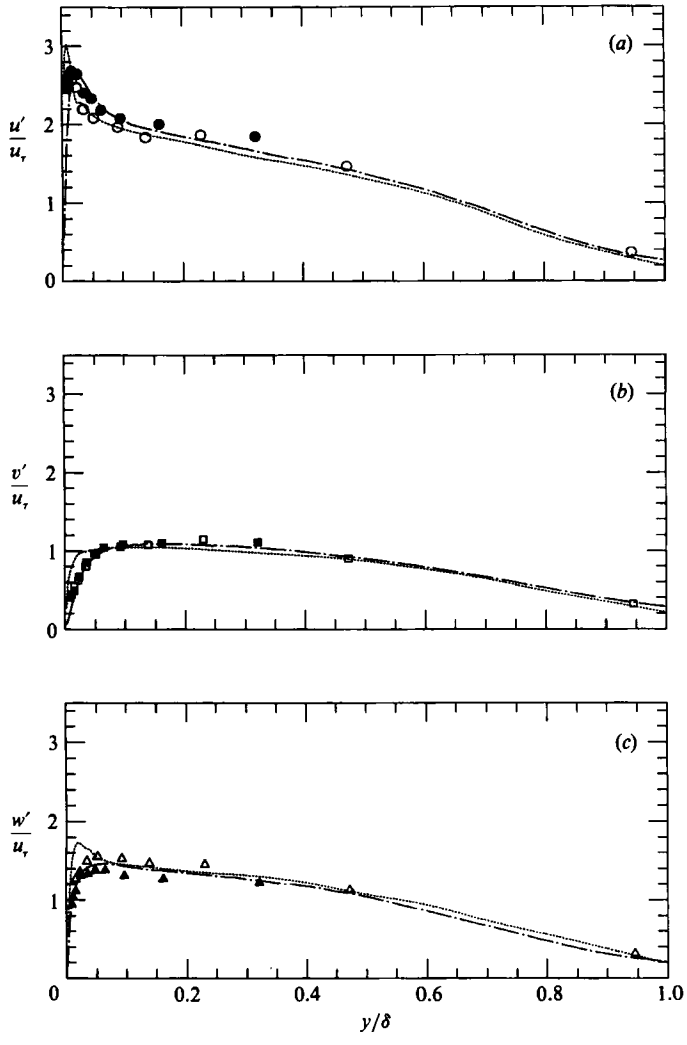

FIGURE 2. Measured r.m.s. fluctuating velocity components normalized with outer scaling u_τ and δ and compared to other measured and simulated values. Symbols given in table 2.

region above $y^+ = 15$ of bounded flows does not exhibit similarity with inner variable scaling at low Reynolds numbers. This dependence on Reynolds number, which was also pointed out by Purtell, Klebanoff & Buckley (1981) and seen by Spalart (1988) for all three r.m.s. velocity components, is also evident in the Kim *et al.* (1987) simulation of the normal fluctuation component shown in figure 3(*b*); it appears to be present for the spanwise component as well, as seen in figure 3(*c*). The measurements of Kastrinakis & Eckelmann (1983) of the normal component do not follow the Reynolds-number trend near the wall. They needed to use correction factors for the cross-stream velocity components which probably did not sufficiently correct the normal component data there.

The normalized third moments or skewness factors of the fluctuating velocity components are shown in figure 4(*a–c*) for the near-wall region. Our present data, as well as the data of Balint *et al.* (1987), agree quite well with those of Wei (1987) for the streamwise component skewness factor $S(u)$ as seen in figure 4(*a*). Wei (1987)

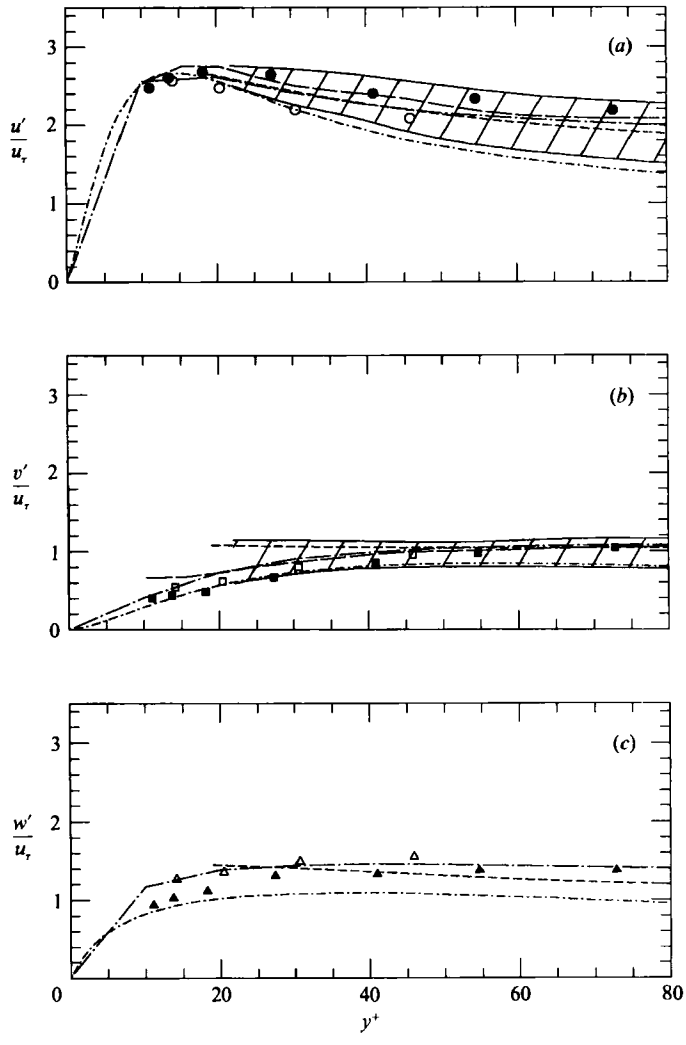

FIGURE 3. Measured r.m.s. fluctuating velocity components normalized with inner scaling u_τ and ν and compared to other measured and simulated values. Symbols given in table 2. Hatched band shows range of Wei & Willmarth (1989) data. Upper bound, $R_{\frac{1}{2}d} = 39582$; lower bound, $R_{\frac{1}{2}d} = 2970$.

does not find a strong Reynolds-number dependence for this statistic. The simulation of Kim *et al.* (1987) and the measurements of Kastrinakis & Eckelmann (1983) of this component are considerably more negative for $y^+ > 15$. The skewness factors of our present data for the normal component $S(v)$ are slightly negative in the region $15 < y^+ < 50$, as shown in figure 4(b), but not so much as in our Balint *et al.* (1987) measurements, which are less reliable because of the greater percentage of unconverged data near the wall, as mentioned above. This negative skewness $S(v)$ is also seen in the data of Wei (1987) and of Kim *et al.* (1987) within the buffer layer but not in the data of Kastrinakis & Eckelmann (1983), which have a high positive skewness, or in those of Klewicki (1989). Klewicki (1989) has tabulated this statistic for numerous investigations and find no consistent trend to explain the rather large differences. Gresko (1988), however, has shown that v-component statistics measured with hot wires are much more subject to measurement errors due to thermal cross-

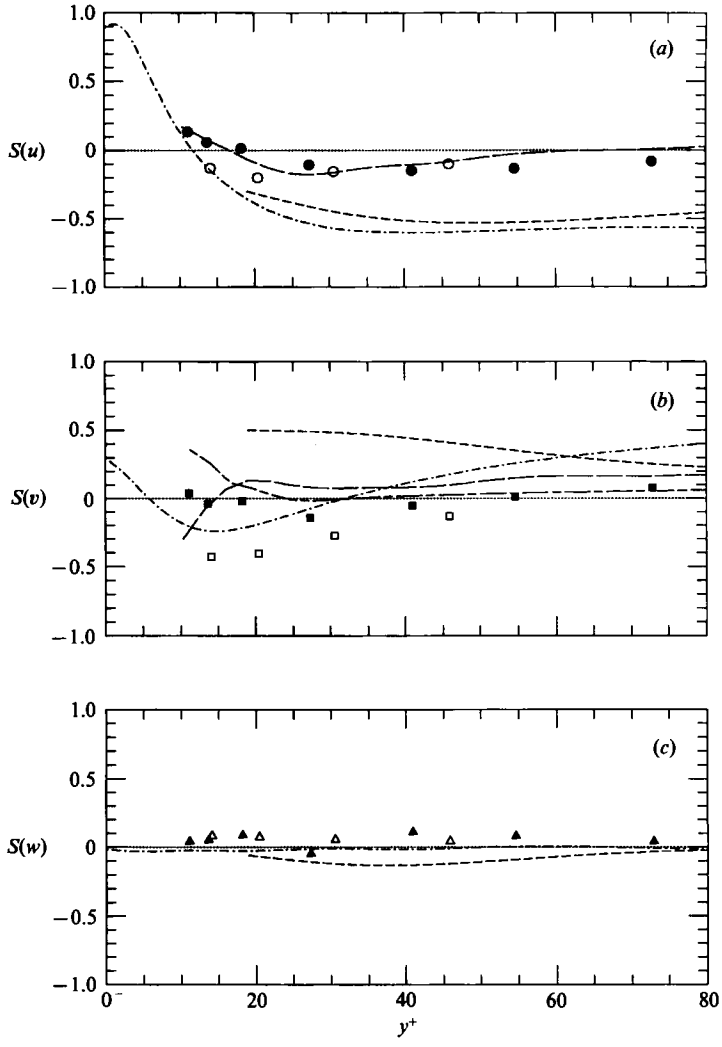

FIGURE 4. Measured skewness factors of fluctuating velocity components compared to other measured and simulated values. Symbols given in table 2.

talk and length-to-diameter sensor wire ratio effects than u-component statistics. Recent highly resolved LDV measurements by Karlsson & Johansson (1988) appear to provide the best values obtained in the laboratory for this statistic. With a resolution of 0.5 viscous lengths in the wall-normal direction in a boundary layer at $R_\theta = 2420$, they obtained values of about -0.2 in the region $y^+ \approx 3$–20, crossing over to positive values at $y^+ \approx 40$ and agreeing very well with the simulation of Kim *et al.* (1987). The skewness factor for the spanwise component $S(w)$ should be zero because of the symmetry of the mean flow. Both our laboratory measurements and those of Kastrinakis & Eckelmann (1983), as well as the simulation of Kim *et al.* (1987) all demonstrate this symmetry reasonably well as seen in figure 4(*c*).

The normalized fourth moments or flatness factors of the three fluctuating velocity components are shown in figure 5(*a–c*), where the value of 3.0 for a Gaussian random variable is also indicated. All the laboratory data and numerical simulations in the

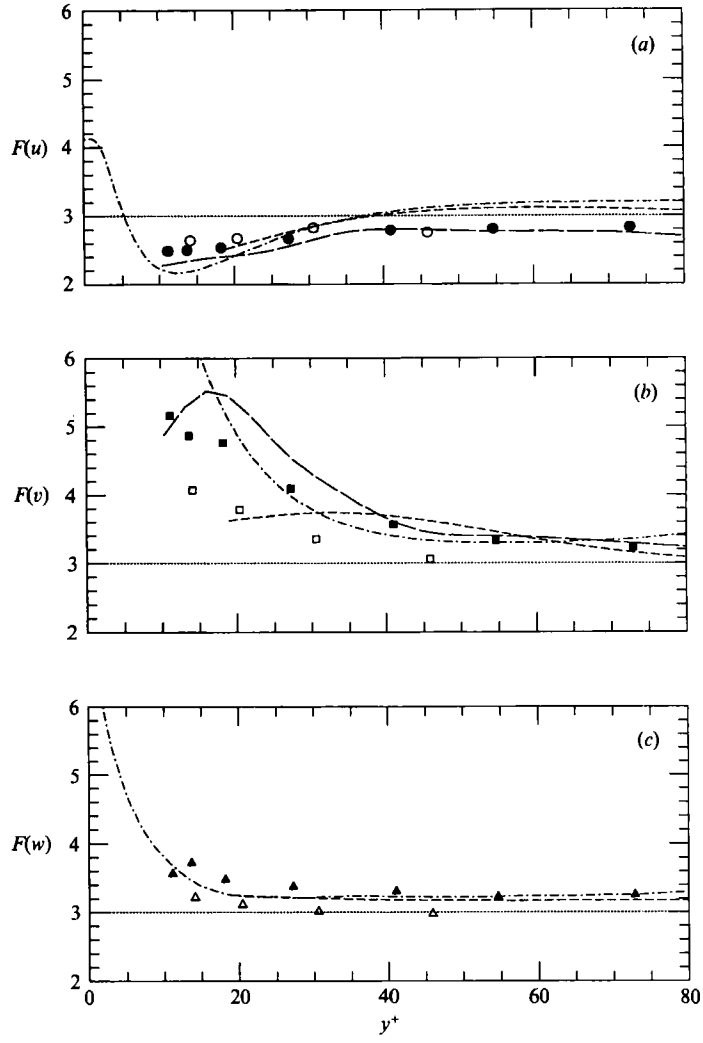

FIGURE 5. Measured flatness factors of fluctuating velocity components compared to other measured and simulated values. Symbols given in table 2.

wall region agree quite well for the streamwise component $F(u)$, as seen in figure 5(*a*). Our present data and those of Balint *et al.* (1987) agree particularly well with those of Wei (1987) at a similar Reynolds number. For the normal component $F(v)$ there is greater variation near the wall as seen in figure 5(*b*). Wei's low-Reynolds-number $F(v)$ (not shown here) increases rapidly with decreasing y^+ in the same manner as the data of Kim *et al.* (1987), possibly indicating a Reynolds-number dependence near the wall. However, the data of Karlsson & Johansson (1988) also show this trend, probably indicating some attenuation of our highest amplitudes of the normal velocity component fluctuations. The flatness factor of the spanwise component $F(w)$ is very similar for all the measurements and the simulation compared in figure 5(*c*).

It should be mentioned that the skewness and flatness factors of the fluctuating velocity components shown in figures 4 and 5 as well as those for the fluctuating vorticity components, later shown in figures 13 and 14, obtained from the database

of Kim *et al.* (1987) have been provided by J. Kim (1989, private communication). He calculated the vorticity component skewness and flatness values for the purposes of this comparison.

3.3. *Reynolds shear stress*

The Reynolds shear stress, normalized by outer variables u_τ^2 (the mean shear stress at the wall) and δ, is compared in figure 6(*a*) to the measurements of Klebanoff (1954) and the simulation values of Spalart (1988). Except for our data point at $y/\delta \approx 0.32$ the agreement is good. The too-large value at that location is also seen for the r.m.s. streamwise component value in figure 2(*a*), and is probably due to the mean velocity at this location not sufficiently matching the mean velocity at which the pitch and yaw calibration was carried out.

In the near-wall region the same data are plotted as a function of y^+ in figure 6(*b*). The Wei & Willmarth (1989) channel flow measurements shows a well-defined increase in the maximum value of the Reynolds shear stress with increasing Reynolds number from a value of about 0.65 at $R_{\frac{1}{2}d} = 2970$ to a value of about 0.88 at $R_{\frac{1}{2}d} = 39582$ as seen in the band hatched in the figure. This again demonstrates the lack of similarity of a turbulent boundary layer at low Reynolds number for inner variable scaling. It should be pointed out that their calculation of the Reynolds shear stress from the momentum equation for channel flow shows that their measurements are somewhat too low in the near-wall region ($y^+ < 80$) at $R_{\frac{1}{2}d} = 22796$; they attribute this to probe resolution. Our data agree reasonably well with their measurements at this comparable Reynolds number for $y^+ < 45$ and are only slightly larger than their calculated values for $y^+ > 45$. This may indicate that our values are also attenuated near the wall because of probe resolution, although this is not seen in the correlation coefficient discussed below. The channel flow data of Kastrinakis & Eckelmann (1983) also agree quite well with Wei & Willmarth (1989) for the smaller y^+ values, but deviate from their results for $y^+ \geqslant 60$. The low-Reynolds-number channel flow data of Kim *et al.* (1987) are in fair agreement with the low-Reynolds-number results of Wei & Willmarth (1989). The values of Spalart (1988) appear to be somewhat too large in the buffer layer when compared to the other results and to the Reynolds-number trend of the Wei & Willmarth (1989) data.

When the Reynolds shear stress is plotted as a correlation coefficient and as a function of y/δ in figure 6(*c*), our values are larger than the measured values of Wei & Willmarth (1989) for $y/\delta < 0.1$ where the boundary layer and channel flows are comparable. However, their computed values from the momentum equation are closer to ours in this region of the flow; at y/δ of 0.1, their measured value is about 10% smaller than their computed value and this percentage becomes greater with decreasing y^+. For $y/\delta > 0.1$ our data show the same trend as the boundary-layer data of Klebanoff (1954), but with a smaller maximum plateau of about 0.44 compared to about 0.5 for Klebanoff (1954). Our values are more consistent with the other data compared. In this region, we agree very well with the boundary-layer simulation of Spalart (1988). Wei (1987) found that the maximum value of the correlation coefficient increases with decreasing Reynolds number from about 0.34 at $R = 39582$ to about 0.44 at $R = 14914$. However, the peak then decreases again to about 0.39 for his lowest Reynolds number of $R = 2970$. With this in mind, the maximum value obtained by Kim *et al.* (1987) at a similarly low Reynolds number is somewhat larger than that found by Wei (1987). The Kastrinakis & Eckelmann (1983) results are lower throughout the wall region than the data of Wei (1987) at a comparable Reynolds number.

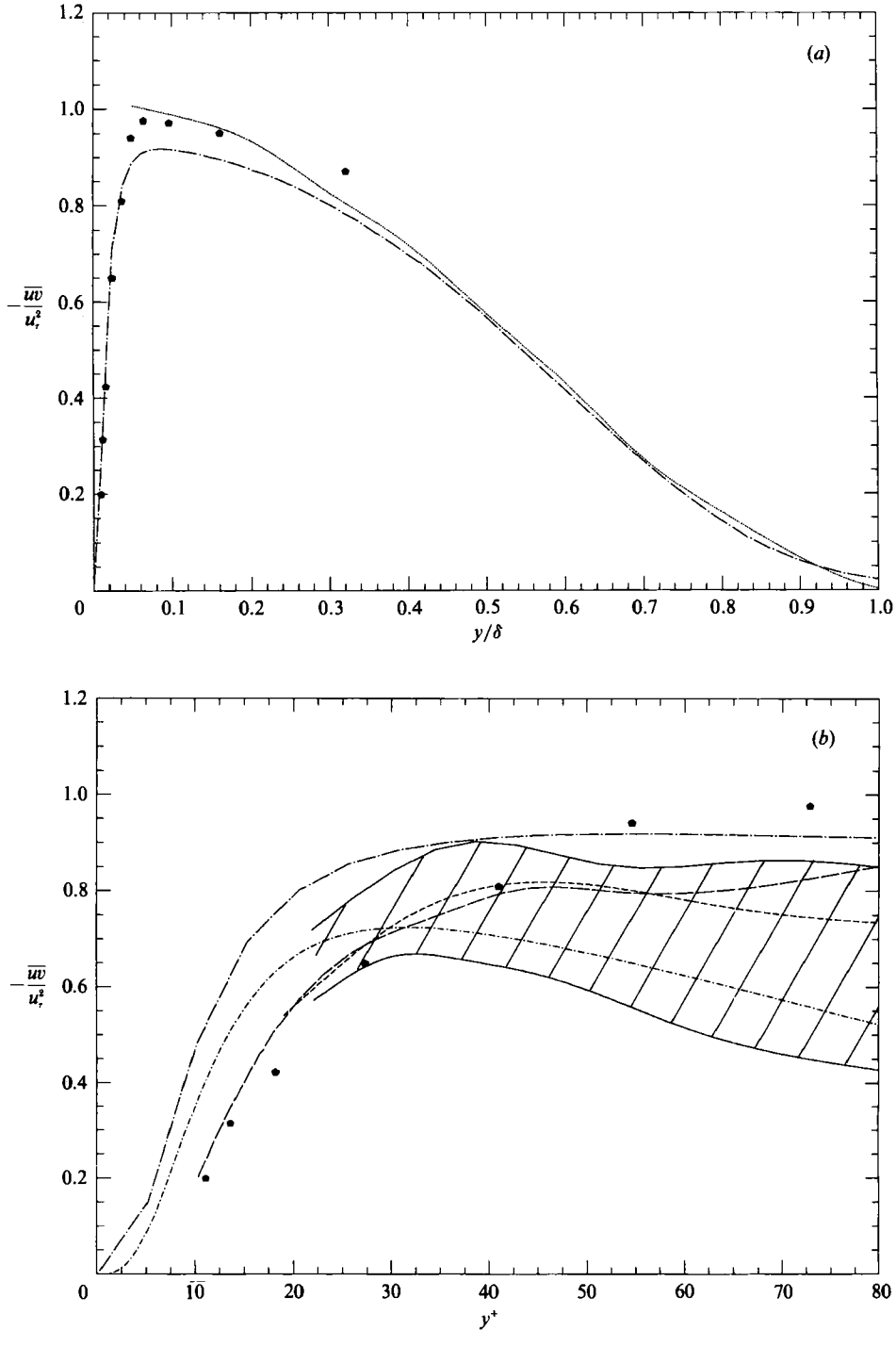

FIGURE 6(a, b). For caption see facing page.

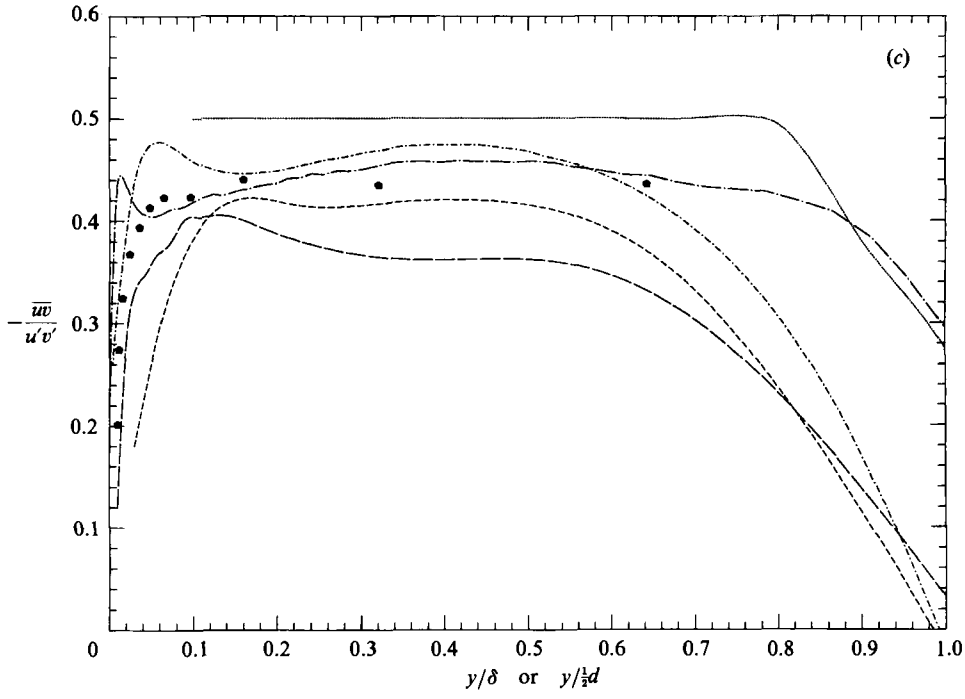

FIGURE 6. (*a*) Measured Reynolds shear stress normalized with outer scaling u_τ and δ and compared to other measured and simulated values. (*b*) Measured Reynolds shear stress normalized with inner scaling u_τ and ν and compared to other measured and simulated values. Shaded band shows range of Wei & Willmarth (1989) data. Upper bound, $R_{\frac{1}{2}d} = 39582$; lower bound, $R_{\frac{1}{2}d} = 2970$. (*c*) Measured Reynolds shear stress correlation coefficient compared to other measured and simulated values. Symbols given in table 2.

3.4. *Velocity spectra*

In figures 7(*a–c*) and 8, the one-dimensional energy spectrum functions

$$\phi(\omega) = E_i(\omega)/\overline{u_i^2}, \tag{2}$$

where

$$\int_0^\infty \phi_i(\omega)\,\mathrm{d}\omega = 1.0, \tag{3}$$

for the three velocity components and the Reynolds shear stress cross-spectrum are shown, normalized with the boundary-layer thickness. The spectra are for $y^+ = 18.3$ in our boundary layer. Here $\omega = 2\pi f$ indicates the angular frequency. The spectra have been plotted as a function of the wavenumber $k_x = \bar{U}/2\pi f$, which is also normalized with δ. These are, in fact, frequency spectra for which the streamwise wavenumbers have been estimated in the usual way using Taylor's hypothesis with the local mean velocity at the point of measurement as the convection velocity. In these figures we compare our measured spectra to frequency spectra of Wei & Willmarth (1989) similarly transformed using Taylor's hypothesis to streamwise wavenumber spectra. Also compared are the true streamwise wavenumber spectra of Spalart (1988). These comparison spectra were obtained at $y^+ = 15.9$ and $y^+ = 15$ respectively. In general there is good agreement between the spectra, particularly between ours and those of Wei & Willmarth (1989). Spalart's (1988) spectra of all three components show a small buildup of energy at the highest wavenumbers. The

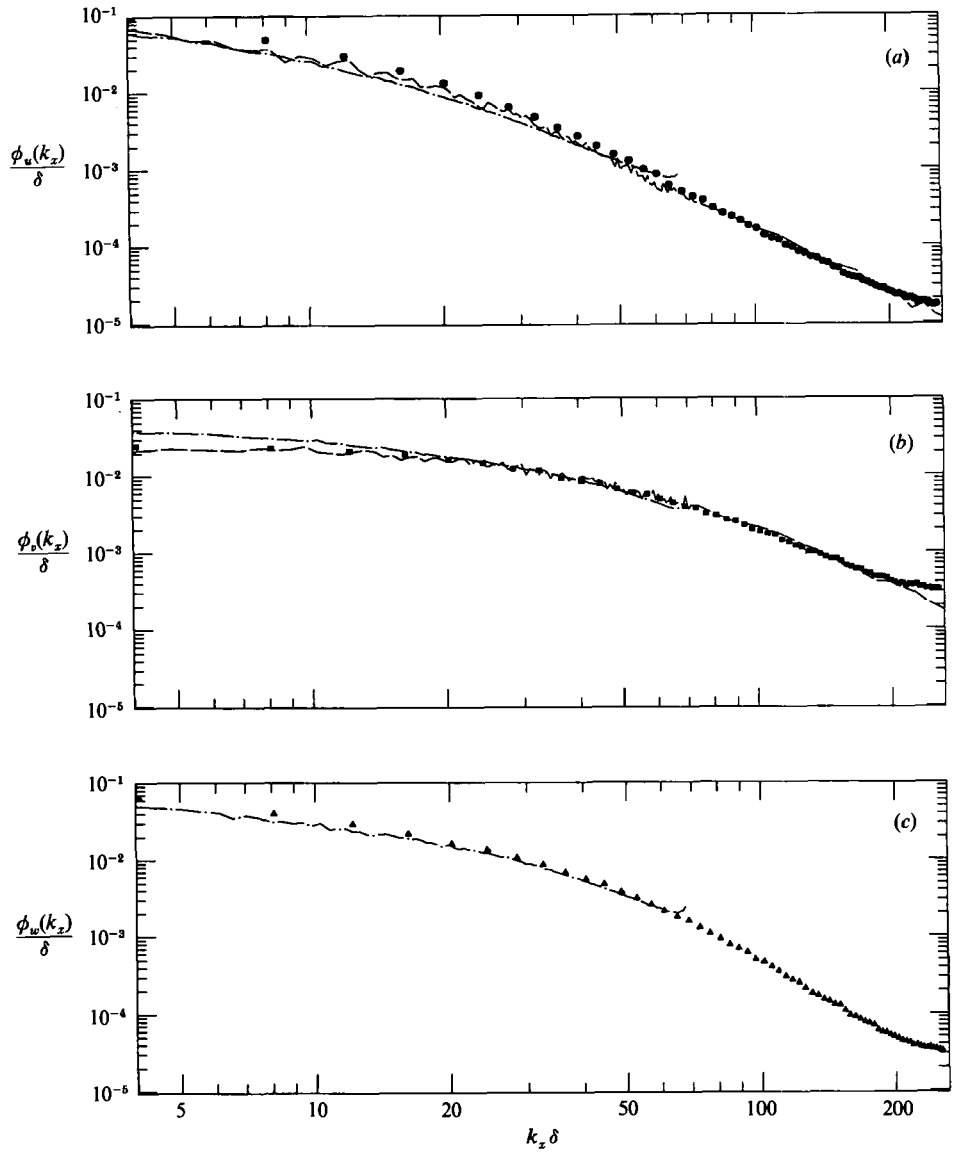

FIGURE 7. Measured one-dimensional fluctuating velocity component spectra at $y^+ = 18$ compared to other measured (Wei & Willmarth 1989 at $y^+ = 15.9$) and simulated (Spalart 1988 at $y^+ = 15$) results. Symbols given in table 2.

agreement at our highest wavenumbers supports our contention in Part 1 that the nine-sensor probe resolves the velocity field quite well. Particularly satisfying is the agreement between Wei & Willmarth (1989) v-component spectrum and our data, given the difficulty in measuring this component well.

Our cross-spectrum of the uv product time series is compared to that of Wei & Willmarth (1989) in figure 8. The agreement is excellent except at the highest wavenumbers where our spectrum shows some buildup of energy. However, this only begins to occur at an energy an order of magnitude lower than the maximum.

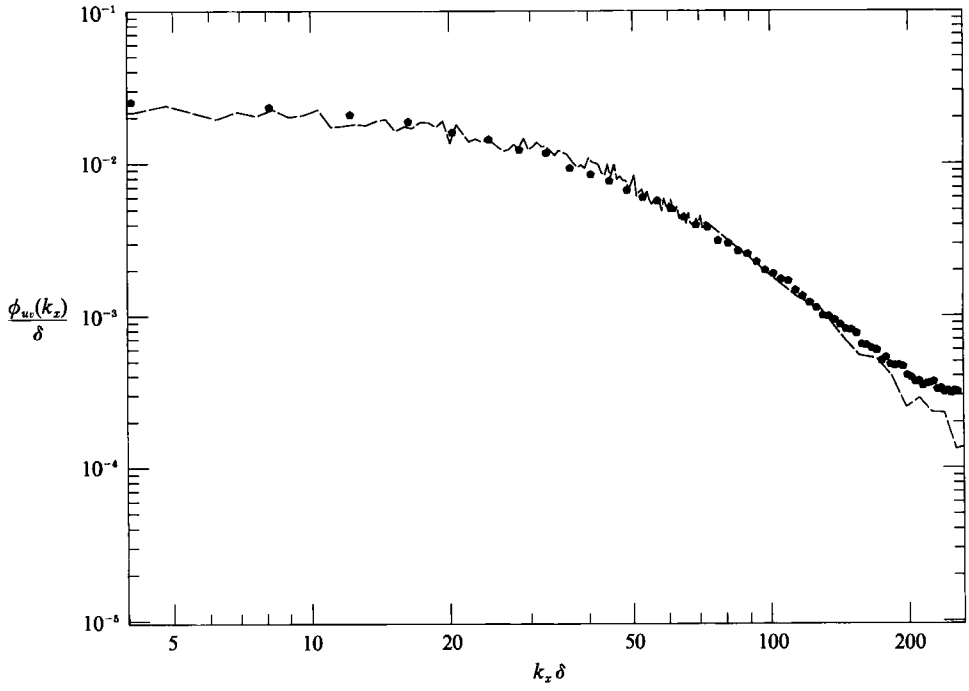

FIGURE 8. Measured one-dimensional uv-product cross-spectrum at $y^+ = 18$ compared to measured results of Wei & Willmarth (1989) at $y^+ = 15.9$. Symbols given in table 2.

3.5. *Turbulent kinetic energy transport*

The transport equation for turbulent kinetic energy is given by

$$\underbrace{\bar{U}_j \frac{\partial}{\partial x_j}(\tfrac{1}{2}\overline{u_i u_i})}_{\text{I}} = \underbrace{-\overline{u_i u_j}\frac{\partial \bar{U}_i}{\partial x_j}}_{\text{II}} \underbrace{-\frac{\partial}{\partial x_j}(\tfrac{1}{2}\overline{u_i u_i u_j})}_{\text{III}} \underbrace{-\frac{1}{\rho}\overline{u_j \frac{\partial p}{\partial x_j}}}_{\text{IV}} + \underbrace{D}_{\text{V}} \underbrace{-\epsilon}_{\text{VI}}. \tag{4}$$

The terms in this equation are clearly interpreted by Corrsin (1953) as

I: the rate of advection of turbulent energy from mean motion kinetic energy;

II: the rate of production of turbulent energy from mean motion kinetic energy;

III: the rate of advection of turbulent energy by turbulent motion;

IV: the rate of transfer of turbulent energy by the work of fluctuating pressure gradients.

Corrsin (1953) points out that the last two terms, which can be combined into a single viscous term, are often misinterpreted. They are correctly defined and interpreted as

V: $D = \nu[\nabla^2(\frac{1}{2}\overline{u_i u_i}) + (\partial^2/\partial x_i \partial x_k)(\overline{u_i u_k})]$, which is the rate of transport (diffusion) of turbulent energy by viscous forces; and

VI: $\epsilon = \overline{\nu(\partial u_i/\partial x_k)[(\partial u_i/\partial x_k) + (\partial u_k/\partial x_i)]}$, which is the rate of dissipation of turbulent energy to heat.

In figure 9 the production and dissipation rate terms measured in our boundary layer are normalized with the outer variables δ and u_τ^3 and plotted as a function of y/δ. They are compared to the previous boundary-layer measurements of Klebanoff (1954) and to the simulation of Spalart (1988). The dissipation rate values of

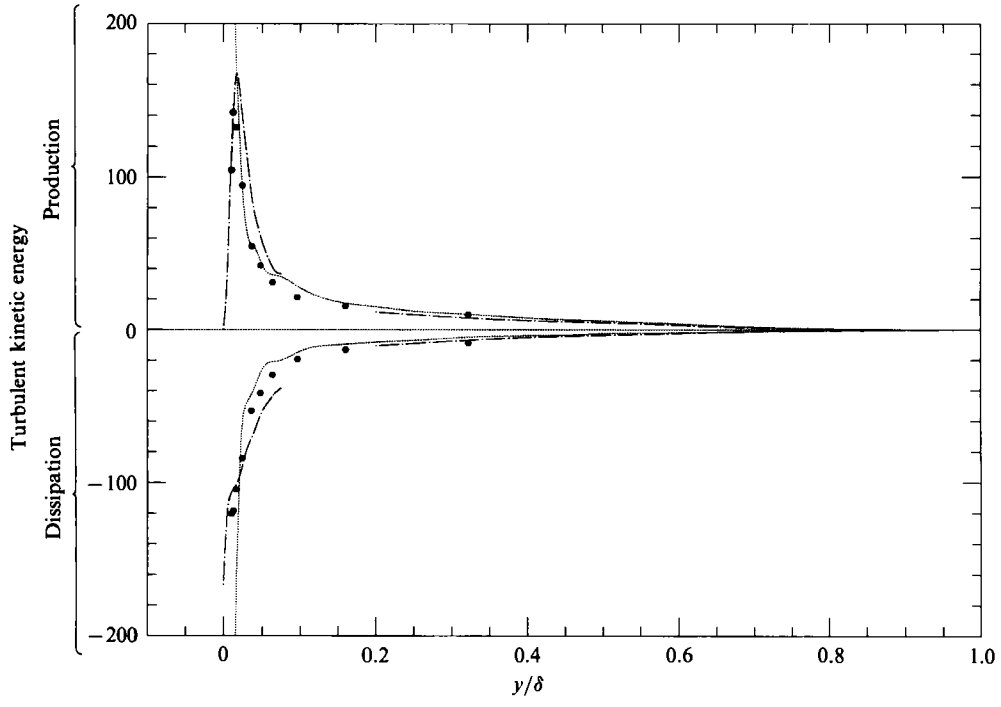

FIGURE 9. Measured turbulent kinetic energy production and dissipation rates normalized with outer scaling u_τ and δ and compared to other measured and simulated values. Symbols given in table 2.

Klebanoff (1954) were found from the three time derivatives $\mathrm{d}u/\mathrm{d}t$, $\mathrm{d}v/\mathrm{d}t$, and $\mathrm{d}w/\mathrm{d}t$, which were transformed to streamwise spatial derivatives with Taylor's hypothesis, and from direct measurements of $\mathrm{d}u/\mathrm{d}y$ and $\mathrm{d}u/\mathrm{d}z$. For the y- and z-gradients of the v- and w-velocity fluctuation components Klebanoff (1954) assumed isotropic relationships. In the outer part of the flow, for $y/\delta > 0.1$, all of the investigations agree quite well, but in the region close to the wall there are very substantial differences. In particular, Klebanoff's (1954) data show extremely high values of both production and dissipation rates compared to our measurements and Spalart's (1988) simulation, with maximum values at 1240 and 910 respectively (off the scale of the figure). The simulation of Spalart (1988) also gives a somewhat larger maximum value of the production rate than our measurements as seen in detail for the near-wall region in figure 10.

The production and dissipation rate terms are emphasized for $y^+ < 80$ in figure 10, where our measurements are normalized with inner variables ν/u_τ^4 and compared to the simulation values of Spalart (1988) and of Mansour *et al.* (1988). The latter data were computed from the simulation of Kim *et al.* (1987). With this normalization, our measured maximum production rate is considerably smaller than those of both the simulations for the three locations near the wall. This reflects the smaller values of Reynolds shear stress we measured, as was seen in figure 6(*b*). As in that figure for Reynolds shear stress, our values of production rate agree very well with the measured values of Wei (1987) for his $R_{\frac{1}{2}d} = 22776$. He states, however, that his measurements underestimate the momentum balance calculation near the wall and attributes this to probe resolution, even though at this Reynolds number the resolution was 2.2 Kolmogorov lengthscales. In this region it is also unclear how

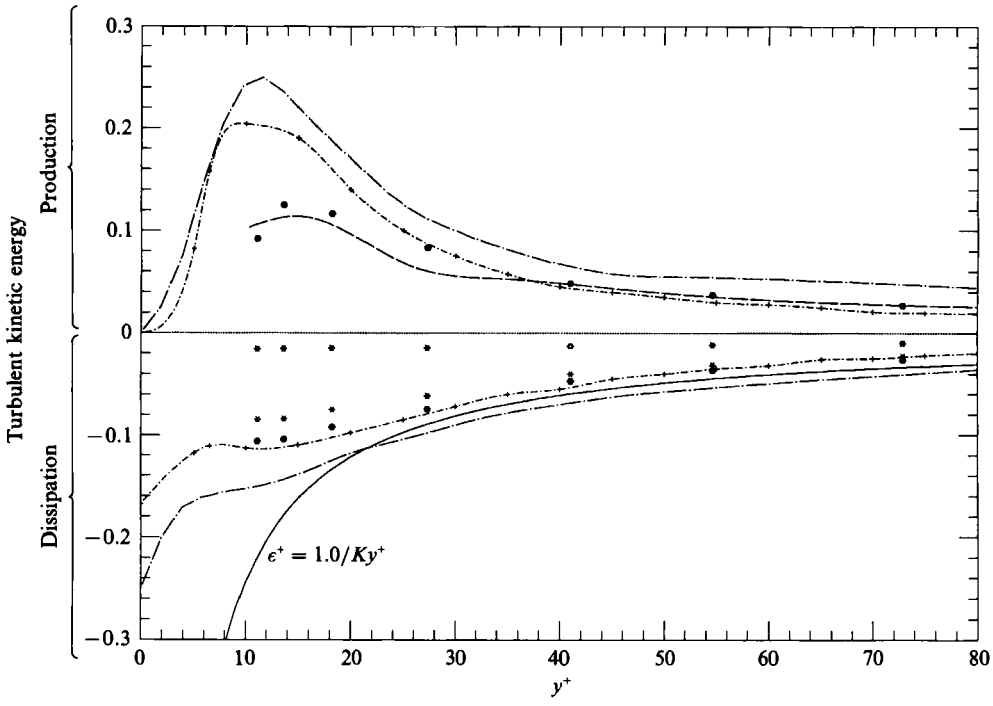

FIGURE 10. Measured turbulent kinetic energy production and dissipation rates normalized with inner scaling u_τ and ν and compared to other measured and simulated values. Symbols given in table 2 except for *, dissipation neglecting cross-product velocity gradient correlations and ✿, dissipation assuming isotropy.

Reynolds-number dependent the data are for inner scaling. Our dissipation rate measurements agree quite well with the computed values of Mansour *et al.* (1988) obtained from the simulation of Kim *et al.* (1987), but are smaller than those of Spalart (1988) near the wall, whose Reynolds number is closer to ours.

Also shown in the figure is the distribution of dissipation rate obtained from our measured streamwise gradient $\partial u/\partial x$ if (*a*) isotropy is assumed,

$$\epsilon = 15\nu\overline{\left(\frac{\partial u}{\partial x}\right)^2}, \tag{5}$$

and if (*b*) the cross-product velocity gradients correlations in the full dissipation rate expression are neglected. It is clear that the flow is extremely anisotropic near the wall, and that the cross-product velocity gradient correlations play an increasingly larger role as the wall is approached.

An estimate of the normalized dissipation rate

$$\epsilon^+ = 1.0/Ky^+ \tag{6}$$

is also shown in figure 10. This expression, given by Tennekes & Lumley (1972), is obtained by assuming that the Reynolds stress in the logarithmic layer is approximately equal to ρu_τ^2, that production equals dissipation rate in this region, and knowing that the gradient of the mean velocity is proportional to u_τ/Ky, where K is the Kármán constant. It is obvious that the estimate in (6) is quite good in the logarithmic region, but it greatly overestimates the dissipation rate in the lower half

of the buffer layer and in the viscous layer where the assumptions in its formulation break down. This fact forced us, in Part 1, to rely on the direct measurements in order to estimate the Kolmogorov lengthscale in the context of the probe resolution discussion.

Although all of these velocity components statistics in §3 have been previously measured and simulated, it is important to assess the capacity of the nine-sensor probe to resolve and measure the velocity field. Moreover, our laboratory velocity measurements take into account, for the first time, the variation of the velocity field over the probe sensing area. If the variation of these velocity statistics with the Reynolds number, as documented by Wei & Willmarth (1989), is taken into consideration, our measurements are in generally good agreement with the highly resolved laboratory results and with the simulations. We do seem to underestimate somewhat the Reynolds stress in the buffer layer and overestimate it in the logarithmic region for inner scaling which is, of course, also reflected in the kinetic energy production rate values obtained with this scaling. These Reynolds stress differences are not so evident, however, when the data are scaled with the outer variables δ and u_τ.

4. Vorticity component statistical properties

Although many of the vorticity component statistics discussed in this section have been determined from direct simulations, many have never been measured in the laboratory. If for no other reason, it is important to show them here in order to verify experimentally the simulations while at the same time verifying the capacity of the nine-sensor probe to measure the vorticity vector. Such verification will provide confidence in measurements made with this probe in more complex turbulent flows which are presently beyond the reach of direct simulations. The new information provided here are the r.m.s. distributions of each of the nine velocity gradients, probability density distributions and spectra of the three vorticity components, and, most importantly, the distribution across the boundary layer of the terms in the enstrophy transport equations.

4.1. *Moments of vorticity fluctuation components*

Our r.m.s. values of all three vorticity components, normalized with outer variables u_τ and δ are shown in figure 11(*a*). These data are compared to our previous boundary-layer measurements, Balint *et al.* (1987), and to the numerical simulation of Spalart (1988). In addition, the r.m.s. of the spanswise component of vorticity ω_z is also compared to the recent laboratory measurements of Klewicki (1989), mentioned earlier. Our spanwise component measurements agree quite well with the measurements of Klewicki (1989) and with the simulation of Spalart (1988). Very near the wall our values are higher than those of Spalart (1988) for the streamwise and normal components with this normalization. In fact, much better collapse of all the data sets for all three components is obtained by scaling with U_∞ and δ as seen in figure 11(*b*). The latter scales the data with a measure of the average shear across the entire boundary layer. It is evident from the figure that the r.m.s. of ω_z is considerably larger near the boundary than are the r.m.s. values of the other two components; the components become much more nearly equal with increasing distance from the wall. This is probably due to spanwise stretching of spanwise vorticity near the wall. As the vortex lines are rotated into the streamwise direction

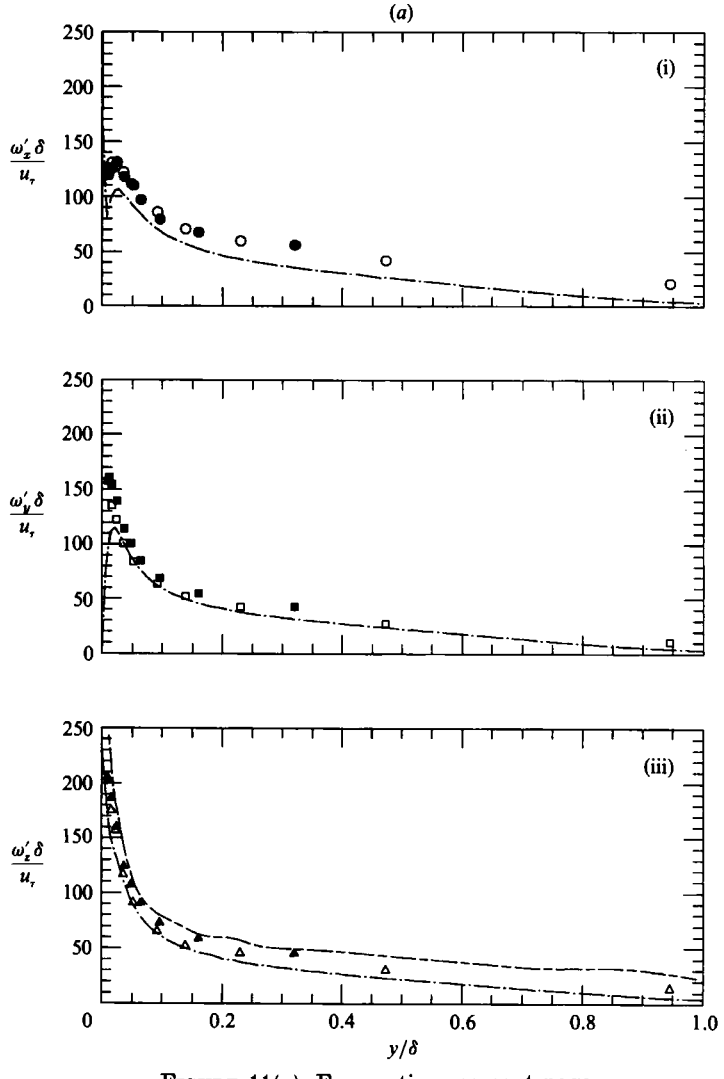

FIGURE 11(*a*). For caption see next page.

and are lifted away from the wall, the r.m.s. values of all three components become nearly equal.

Details of the near-wall region, $y^+ < 80$, are shown in figure 12 where the normalization is with inner variables u_τ and ν. The channel flow measurements of Kastrinakis & Eckelmann (1983) and the simulation of Kim *et al.* (1987) are added to the comparison data for this region of the flow. With this scaling, all three components of vorticity measured in our experiment show somewhat lower values over the wall region than all of the comparison data, particularly for the normal component ω_y. Our new data compares well with our previous data, Balint *et al.* (1987), except for the locations closest to the wall where we now measure somewhat lower values at our higher Reynolds number. Recall that Balint *et al.* (1987) also had a greater problem with obtaining converged solutions in this region as discussed in §3.1. Near the wall there are rather larger differences of almost 30% between the two simulations for the r.m.s. of the streamwise component ω_x. It remains to be

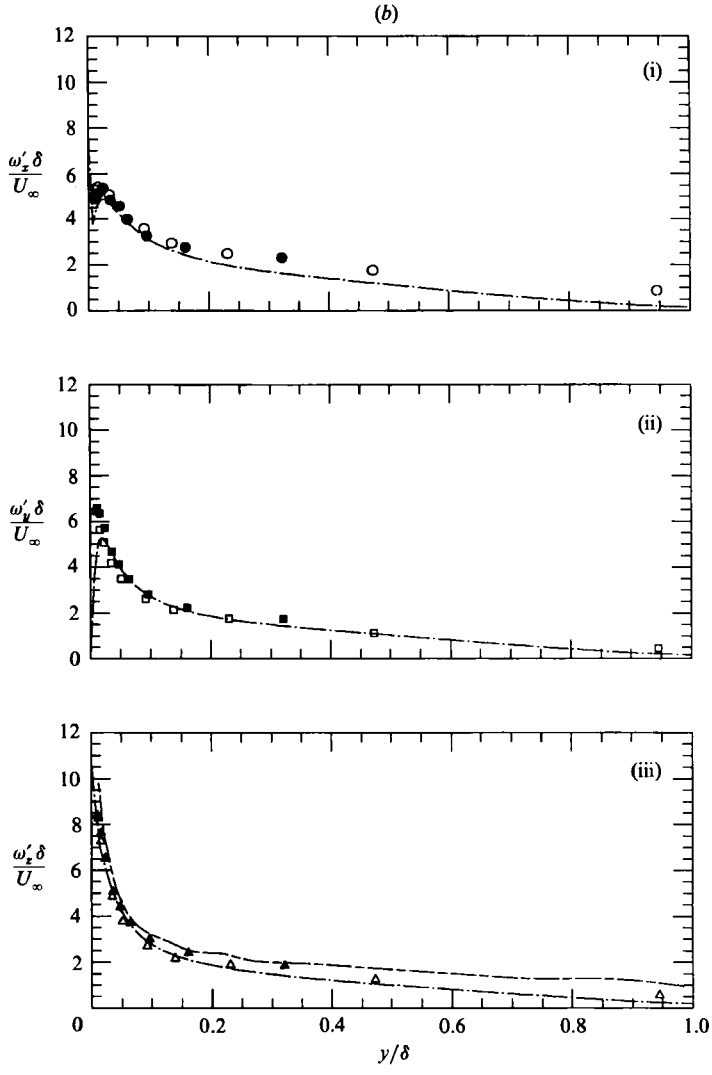

FIGURE 11. (*a*) Measured r.m.s. fluctuating vorticity components normalized with outer scaling u_τ and δ and compared to other measured and simulated values. (*b*) Measured r.m.s. fluctuating vorticity components normalized with variables U_∞ and δ and compared to other measured and simulated values. Symbols given in table 2.

determined whether these differences are primarily due to Reynolds-number dependence, which Spalart's (1988) data at different Reynolds number indicate is in part the case, or whether they are mostly due to measurement and numerical resolution and other errors.

The normalized third and fourth moments, or skewness and flatness factors of the vorticity components, are shown in figures 13 and 14 for the near-wall region. They are compared to the simulation of Kim *et al.* (1987) from which these statistics were computed by J. Kim (1989, private communication). For the streamwise component our data are also compared to the measurements of Kastrinakis & Eckelmann (1983), and for the spanwise component, to the measurements of Klewicki (1987). The skewness of the streamwise and normal components $S(\omega_x)$ and $S(\omega_y)$ should be zero

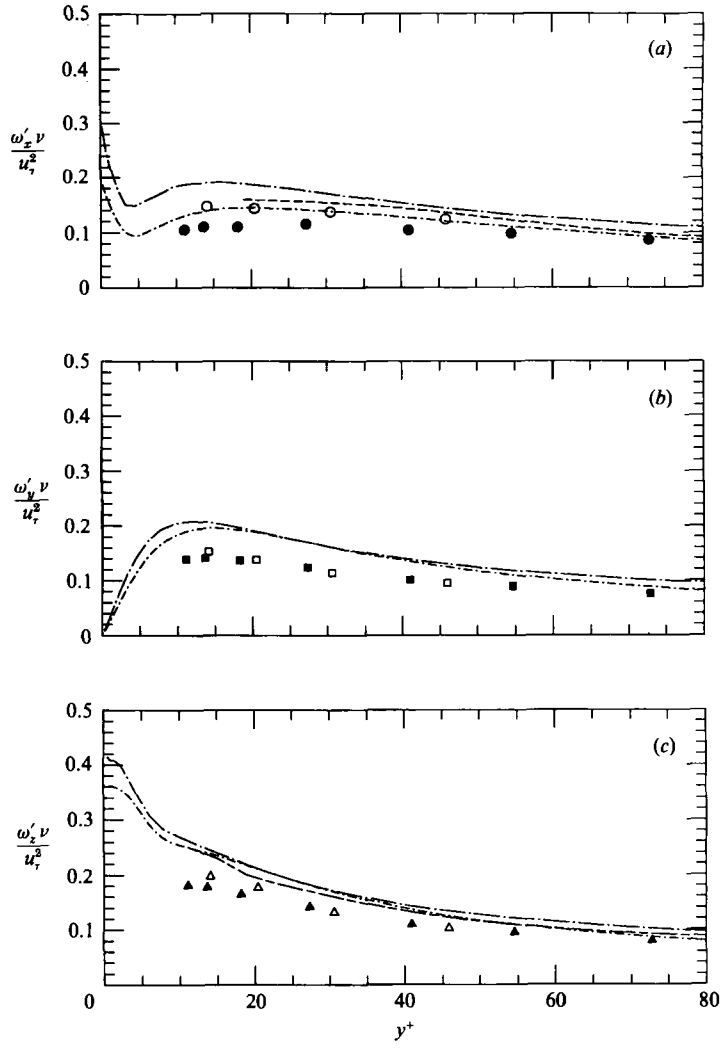

FIGURE 12. Measured r.m.s. fluctuating vorticity components normalized with inner scaling u_τ and ν and compared to other measured and simulated values. Symbols given in table 2.

because of the symmetry of the flow about these axes. The values computed by Kim exhibit these properties quite well; the small deviations are attributed by him to the smaller sample size used to calculate this statistic than was used for the r.m.s. calculations. Our data show good symmetry except for the three points closest to the wall for the streamwise component ω_x. The skewness data of Kastrinakis & Eckelmann (1983) for this component also show considerably asymmetry as the wall is approached, whereas the data of Balint *et al.* (1987) show relatively good symmetry. When the probability density distribution of ω_x is discussed below, it will be seen that this negative skewness in the present data very near the wall is due to small biases in the low-amplitude fluctuations and not because of strong asymmetry of most of the distribution.

The spanwise component of vorticity ω_z is not symmetric; it is quite negatively skewed in the wall region. All of the data sets compared agree rather well for this

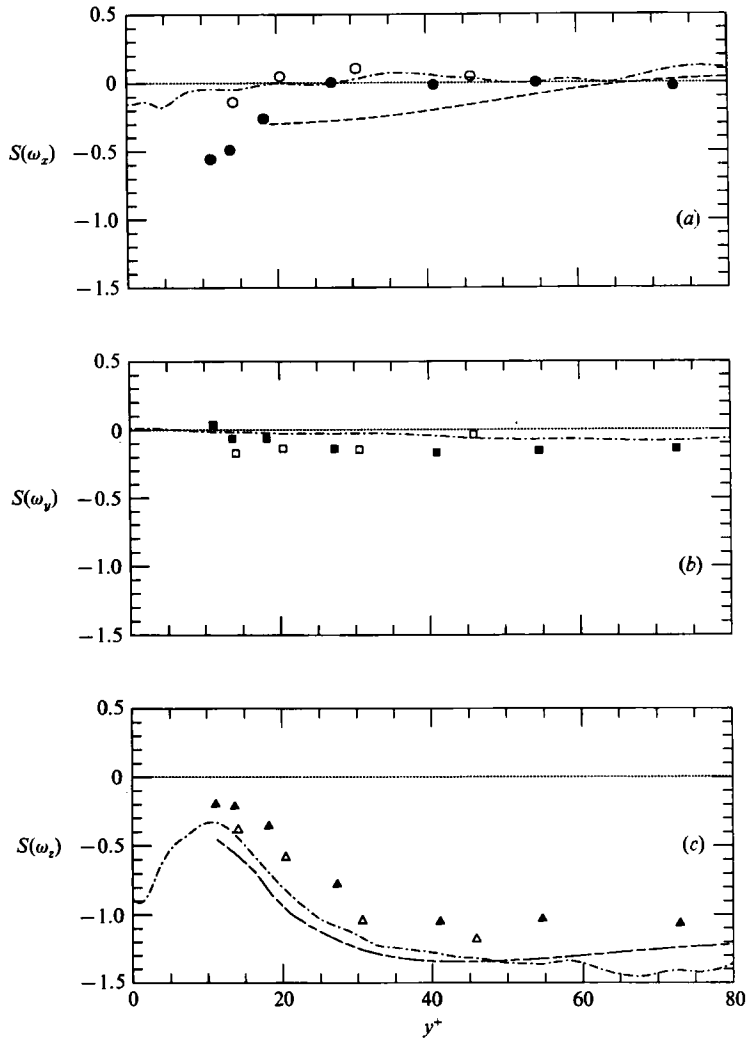

FIGURE 13. Measured skewness factors of fluctuating vorticity components compared to other measured and simulated values. Symbols given in table 2.

statistic. A negative skewness implies that there is higher probability of large negative than of large positive fluctuations, and these negative fluctuations have the same sense of rotation as the mean shear. This indicates that intense vorticity stretching in the spanwise direction is apparently more frequent than compression of the same magnitude, resulting in these skewed distributions.

In figure 14 the flatness factor of 3.0 for a Gaussian random variable is indicated for reference. The flatness factors of all three vorticity components are considerably larger than the Gaussian value except for the normal and spanwise components $F(\omega_y)$ and $F(\omega_z)$ quite close to the wall. This is an indication of the intermittent character of vorticity fluctuations above the buffer layer. Our streamwise component data have substantially smaller values close to the wall than those provided by Kim but are larger than the channel flow data of Kastrinakis & Eckelmann (1983) which are taken at a higher Reynolds number than the simulation but lower than our

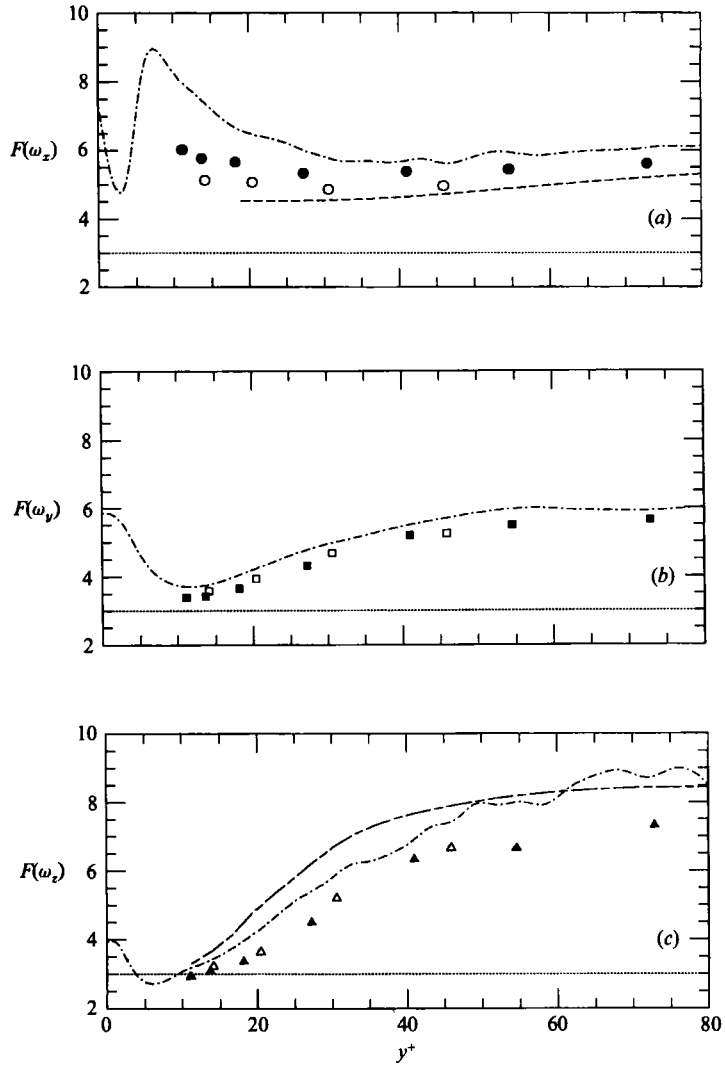

FIGURE 14. Measured flatness factors of fluctuating vorticity components compared to other measured and simulated values. Symbols given in table 2.

experiment. All the data sets agree rather well for the flatness factors of the normal component. Our data are somewhat smaller than both the Kim simulation data and the measurements of Klewicki (1989) for the spanwise component. The slight lack of smoothness of the Kim data is again attributed by him to the smaller data sample used to compute this statistic. Our lower values of the flatness factor for all three vorticity components may be due to probe resolution. This would tend to attenuate the highest-amplitude fluctuations which are heavily weighted in the flatness factor.

The r.m.s. values of the individual velocity gradients, normalized with outer variables, are shown in figure 15. As expected, the cross-stream gradients $\partial/\partial y$ and $\partial/\partial z$ for all these velocity components are significantly larger near the wall than are the streamwise gradients $\partial/\partial x$ which use Taylor's hypothesis. The near-wall-region data, normalized with inner variables, are shown in figure 16. In and above the buffer layer our r.m.s. values of the streamwise gradients compare fairly well with those of

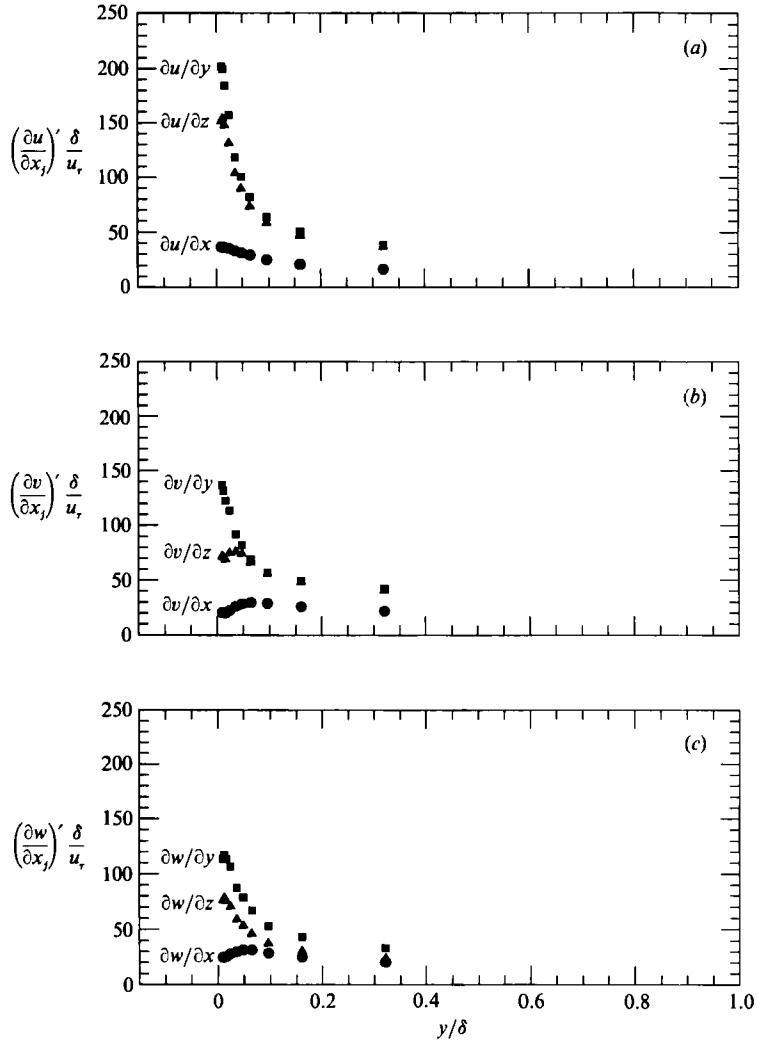

FIGURE 15. Measured r.m.s. fluctuating velocity gradient components normalized with outer scaling u_τ and δ. Symbols given in table 2.

Kim as has been shown by Piomelli *et al.* (1989). This fact supports the use of Taylor's hypothesis as noted in Part 1 and indicates the relatively smaller importance of these streamwise gradients compared to the cross-streamwise gradients in the statistics of the ω_y and ω_z components.

4.2. *Probability density distributions*

The probability density functions (PDFs) of the three vorticity components are shown in figure 17 (*a–c*) for all the measurement locations. Superimposed on these PDFs at $y^+ = 41$, in figure 18, are the PDFs taken in the free stream where the flow is nominally irrotational. The PDFs for the free stream have been previously discussed in Part 1. From figure 18 it is evident that the maximum values of the vorticity components are very much larger than the largest values of spurious vorticity components arising from facility and instrumentation system errors. The

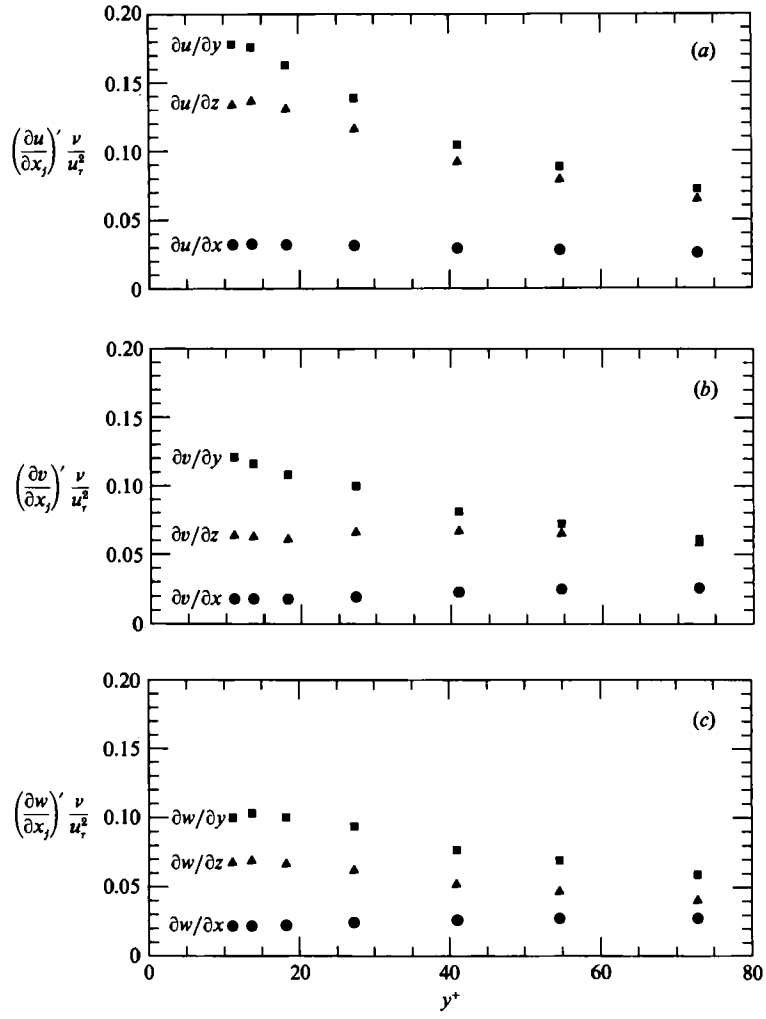

FIGURE 16. Measured r.m.s. fluctuating velocity gradient components normalized with inner scaling u_τ and ν. Symbols given in table 2.

previously determined negative skewness of the spanwise component of vorticity near the wall is quite evident from figure 17(*c*), as is the narrowing of the range of vorticity component values with distance from the wall, a fact reflected in the decrease in the r.m.s. values. The erroneous negative skewness of the streamwise vorticity near the wall seems to be a small bias toward the positive low-amplitude fluctuations combined with the relative narrowness of the distribution, a fact demonstrated by the high flatness of this component. The low-amplitude fluctuations have relatively more weight in the skewness factor for a narrow distribution. The shape of the full PDFs of ω_x very near the wall are not asymmetric in the same obvious manner as those for ω_z in this region, although erroneous negative skewness values of ω_x are even larger there than the negative skewness values of ω_z.

4.3. *Vorticity spectra*

One-dimensional spectra of the three vorticity components at $y^+ = 18$, normalized

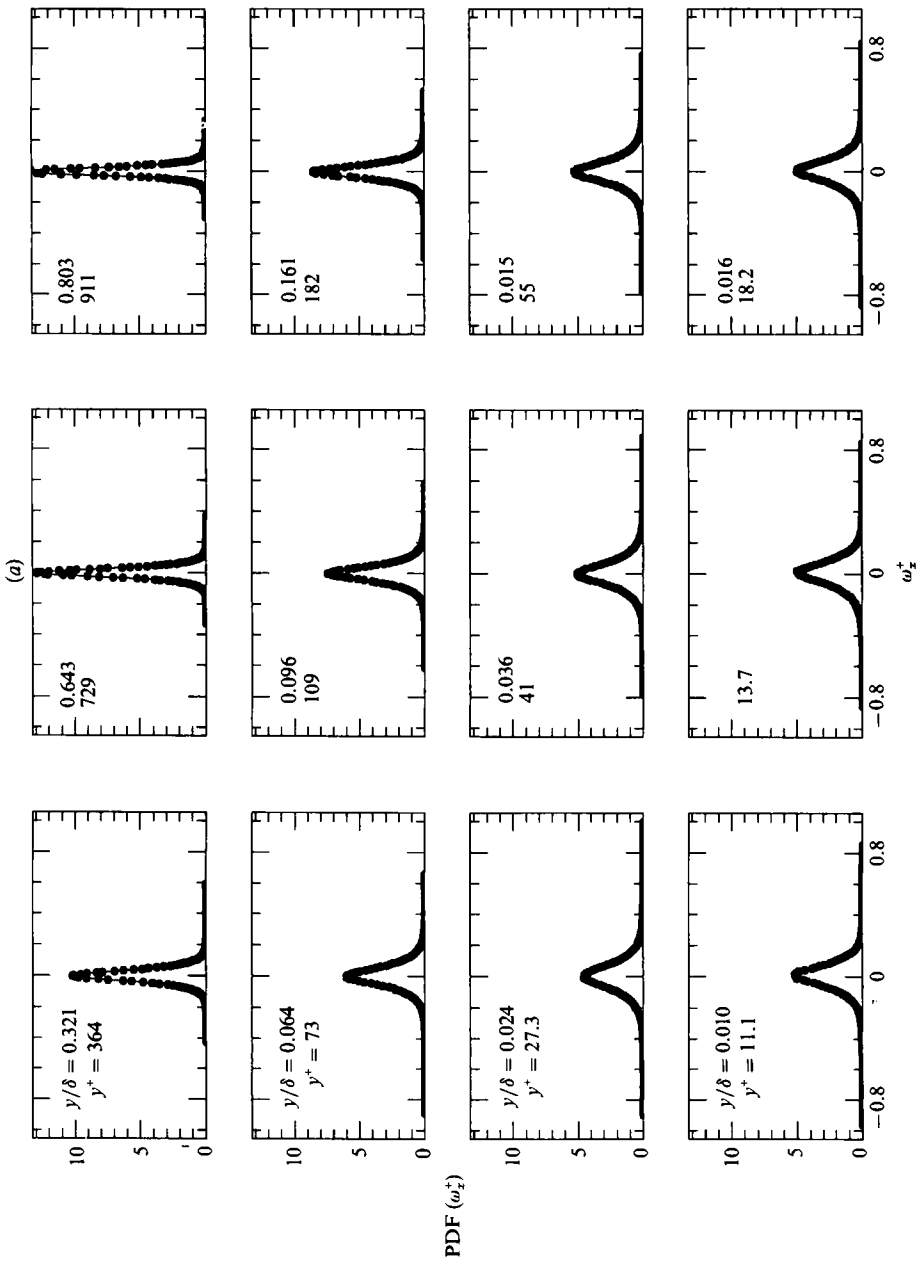
(a)
PDF (ω_z^+)
ω_z^+
$y/\delta = 0.321$
$y^+ = 364$
$y/\delta = 0.064$
$y^+ = 73$
$y/\delta = 0.024$
$y^+ = 27.3$
$y/\delta = 0.010$
$y^+ = 11.1$
0.643
729
0.096
109
0.036
41
13.7
0.803
911
0.161
182
0.015
55
0.016
18.2
10
5
0
−0.8
0
0.8

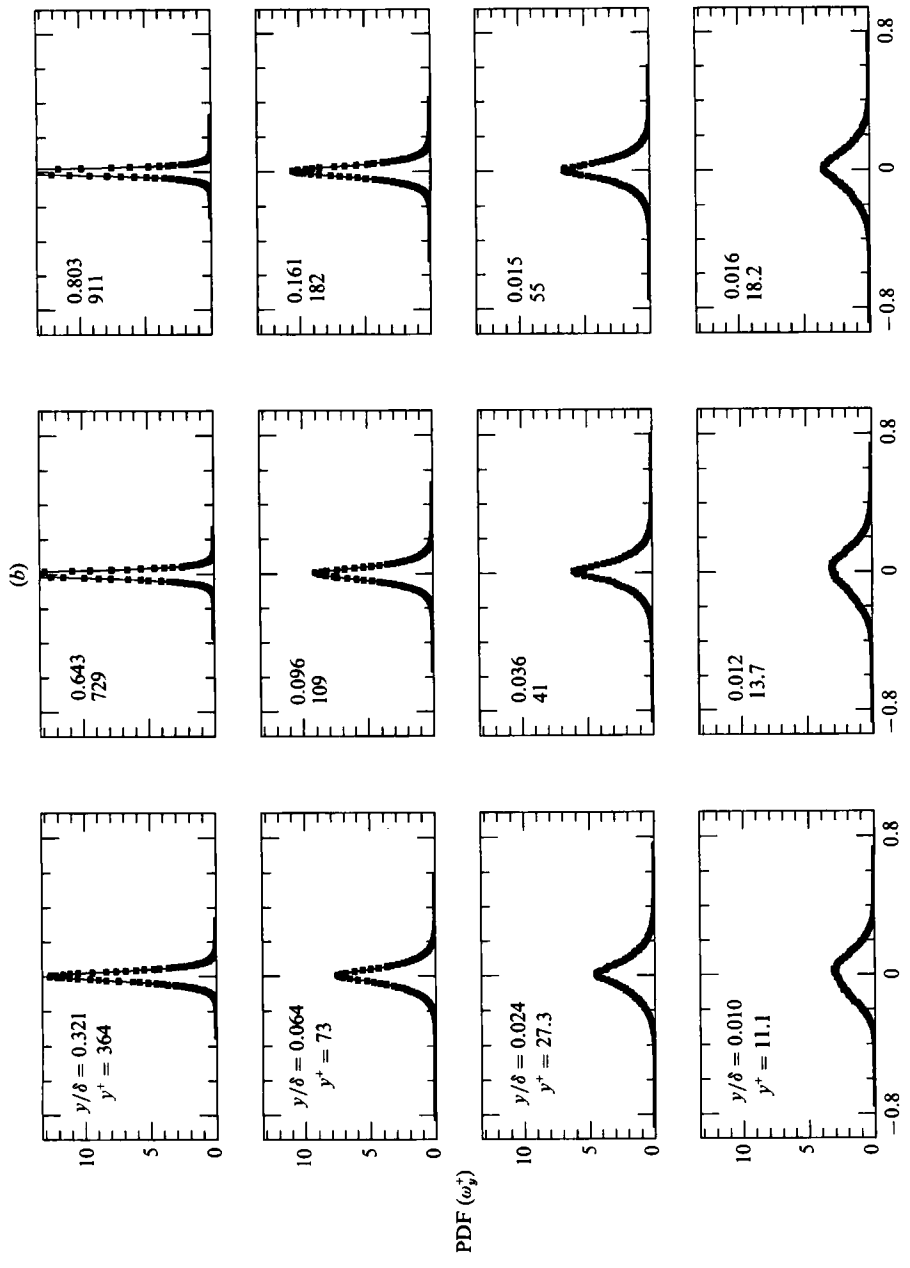

FIGURE 17(*a*, *b*). For caption see next page.

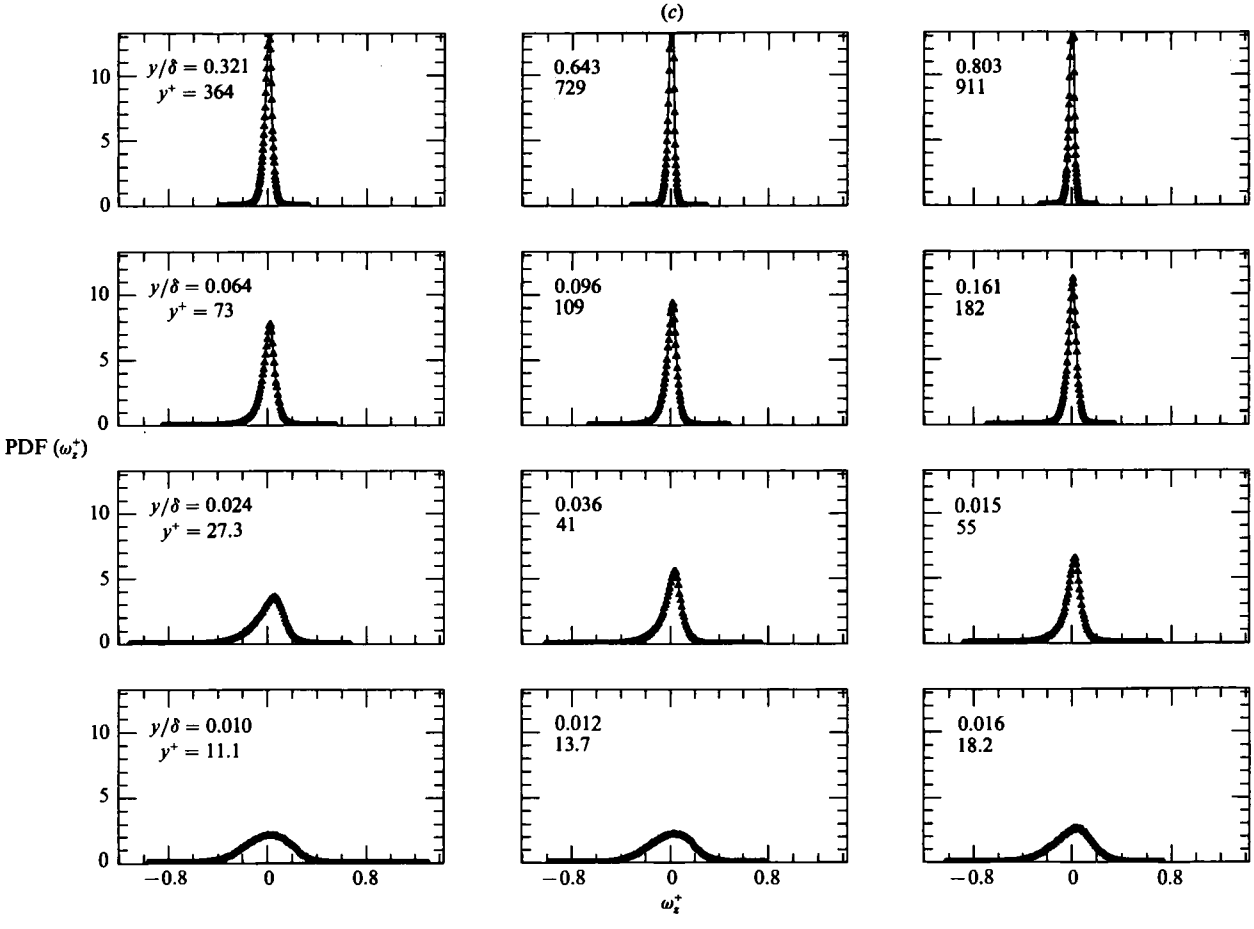

FIGURE 17. Measured probability density functions of the fluctuating vorticity normalized with inner scaling u_τ and ν at positions across the boundary layer. Symbols given in table 2.

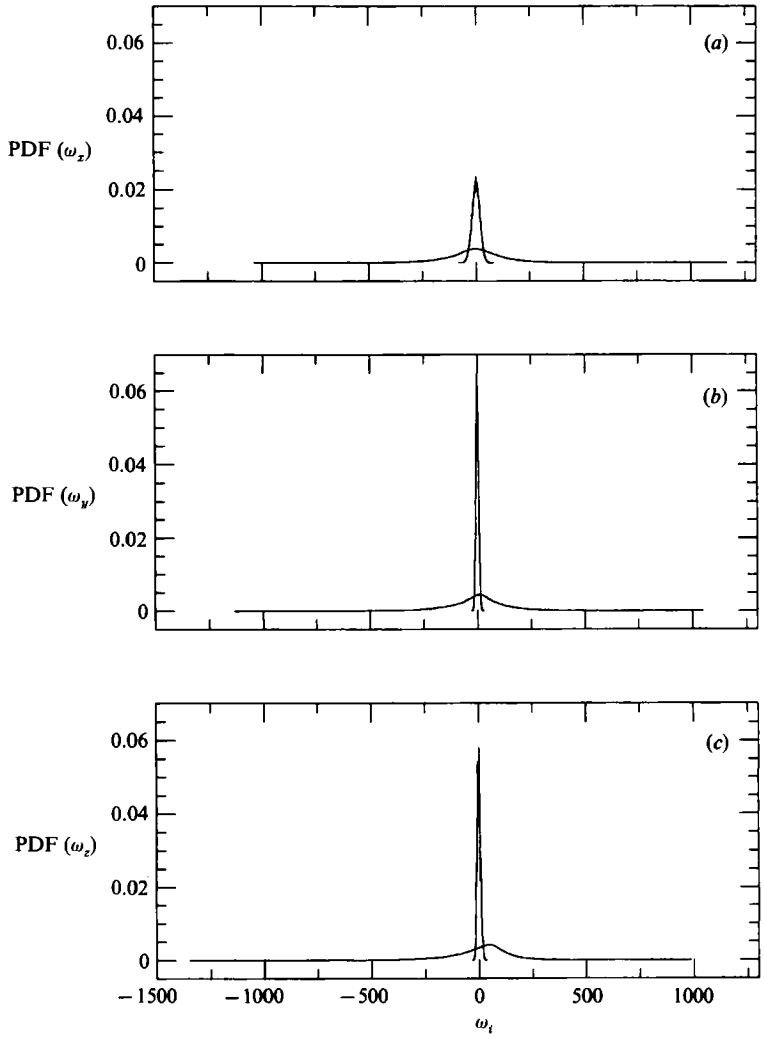

FIGURE 18. Comparison of the measured probability density functions of the fluctuating vorticity components at $y^+ = 41$ and in the free stream where the flow is nominally irrotational.

with the boundary-layer thickness are shown in figure 19(*a–c*). The angular frequencies of our data have again been transformed into streamwise wavenumbers utilizing Taylor's hypothesis. Our measured frequency spectra are compared to the true wavenumber spectra of P. R. Spalart (1990, private communication) at $y^+ = 15$ computed from his $R_\delta = 14500$ boundary-layer database. Except at Spalart's highest wavenumbers, the agreement is very good; all of Spalart's spectra show some buildup of energy at his highest wavenumbers. The energy buildup at high wavenumbers in Spalart spectra is worse for ϕ_{ω_y} and ϕ_{ω_z} which involve his poorest-resolved gradients, i.e. those in the streamwise direction. Our data are also somewhat attenuated at higher wavenumbers because of not adequately resolving the very smallest velocity gradient scales near the wall. The enstrophy (one half of the mean-square vorticity component sum) spectrum is weighted by wavenumber and compared to the kinetic energy spectrum in figure 20. It is evident that the maximum energy occurs at a higher wavenumber for the enstrophy spectrum compared to the

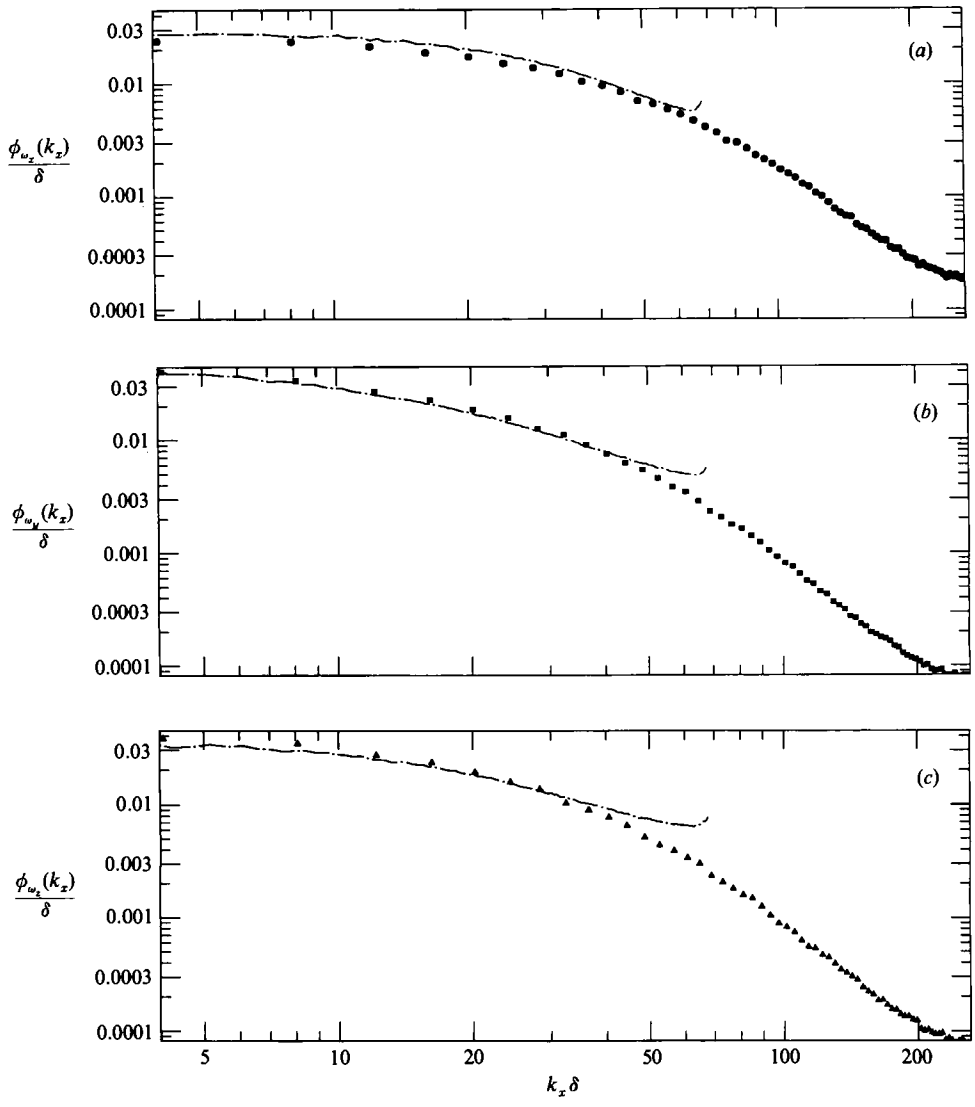

FIGURE 19. Measured one-dimensional fluctuating vorticity component spectra at $y^+ = 18$ compared to direct numerical simulations of P. R. Spalart (1990, private communication) at $y^+ = 15$.

kinetic energy spectrum as expected, but the wavenumber separation at this Reynolds number is not very great.

4.4. *Enstrophy transport*

Balint, Vukuslavčević & Wallace (1990) were the first to determine the terms in the total, mean, and fluctuating enstrophy transport equations for a boundary layer. The equation for the transport of total enstrophy is given by

$$\underbrace{\overline{U_j \frac{\partial}{\partial x_j}(\tfrac{1}{2}\Omega_i \Omega_i)}}_{\text{I}} = \underbrace{\overline{\Omega_i \Omega_j \frac{\partial U_i}{\partial x_j}}}_{\text{II}} + \underbrace{\nu \frac{\overline{\partial^2(\tfrac{1}{2}\Omega_i \Omega_i)}}{\partial x_j \partial x_j}}_{\text{III}} - \underbrace{\nu \overline{\left(\frac{\partial \Omega_i}{\partial x_j}\frac{\partial \Omega_i}{\partial x_j}\right)}}_{\text{IV}}, \tag{7}$$

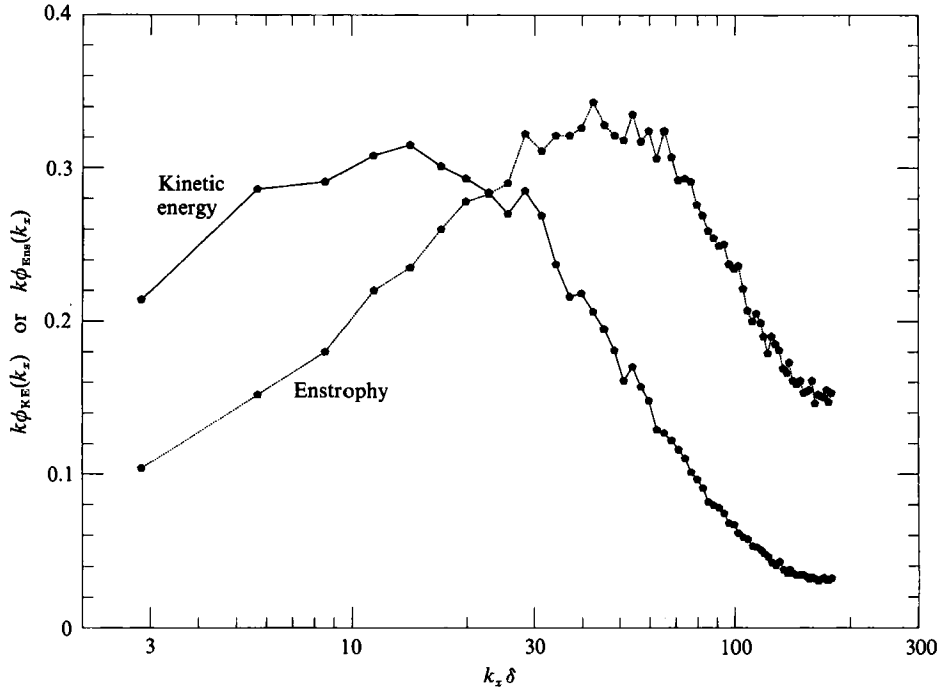

FIGURE 20. Enstrophy spectrum weighted by wavenumber and compared to the kinetic energy spectrum at $y^+ = 18$.

where the four terms are

I: the rate of advection of total enstrophy;

II: the rate of rotation and stretching/compression of total enstrophy by the velocity gradient field;

III: the rate of viscous diffusion of total enstrophy; and

IV: the rate of viscous dissipation of total enstrophy.

As Balint *et al.* (1990) point out, the terms in (7) can be obtained from combinations of the terms in the transport equations for mean and fluctuating enstrophy. These equations are respectively

$$\underbrace{\bar{U}_j\frac{\partial}{\partial x_j}(\tfrac{1}{2}\bar{\Omega}_i\bar{\Omega}_i)}_{\text{I}}+\underbrace{\Omega_i\overline{u_j\frac{\partial\omega_i}{\partial x_j}}}_{\text{II}}=\underbrace{\bar{\Omega}_i\bar{\Omega}_j\frac{\partial\bar{U}_i}{\partial x_j}}_{\text{III}}+\underbrace{\bar{\Omega}_i\overline{\omega_j\frac{\partial u_i}{\partial x_j}}}_{\text{IV}}+\underbrace{\nu\frac{\partial^2(\tfrac{1}{2}\bar{\Omega}_i\bar{\Omega}_i)}{\partial x_j\partial x_j}}_{\text{V}}-\underbrace{\nu\overline{\left(\frac{\partial\bar{\Omega}_i}{\partial x_j}\right)\left(\frac{\partial\bar{\Omega}_i}{\partial x_j}\right)}}_{\text{VI}} \tag{8}$$

and

$$\underbrace{\bar{U}_j\frac{\partial}{\partial x_j}(\tfrac{1}{2}\overline{\omega_i\omega_i})}_{\text{I}}+\underbrace{\overline{u_j\frac{\partial}{\partial x_j}(\tfrac{1}{2}(\omega_i\omega_i)}}_{\text{II}}+\underbrace{\overline{u_j\omega_i}\frac{\partial\bar{\Omega}_i}{\partial x_i}}_{\text{III}}$$

$$=\underbrace{\overline{\omega_i\omega_j}\frac{\partial\bar{U}_i}{\partial x_j}}_{\text{IV}}+\underbrace{\overline{\omega_i\omega_j\frac{\partial u_i}{\partial x_j}}}_{\text{V}}+\underbrace{\bar{\Omega}_j\overline{\omega_i\frac{\partial u_i}{\partial x_j}}}_{\text{VI}}+\underbrace{\nu\frac{\partial^2}{\partial x_j\partial x_j}(\tfrac{1}{2}\overline{\omega_i\omega_i})}_{\text{VII}}-\underbrace{\nu\overline{\left(\frac{\partial\omega_i}{\partial x_j}\right)\left(\frac{\partial\omega_i}{\partial x_j}\right)}}_{\text{VIII}}. \tag{9}$$

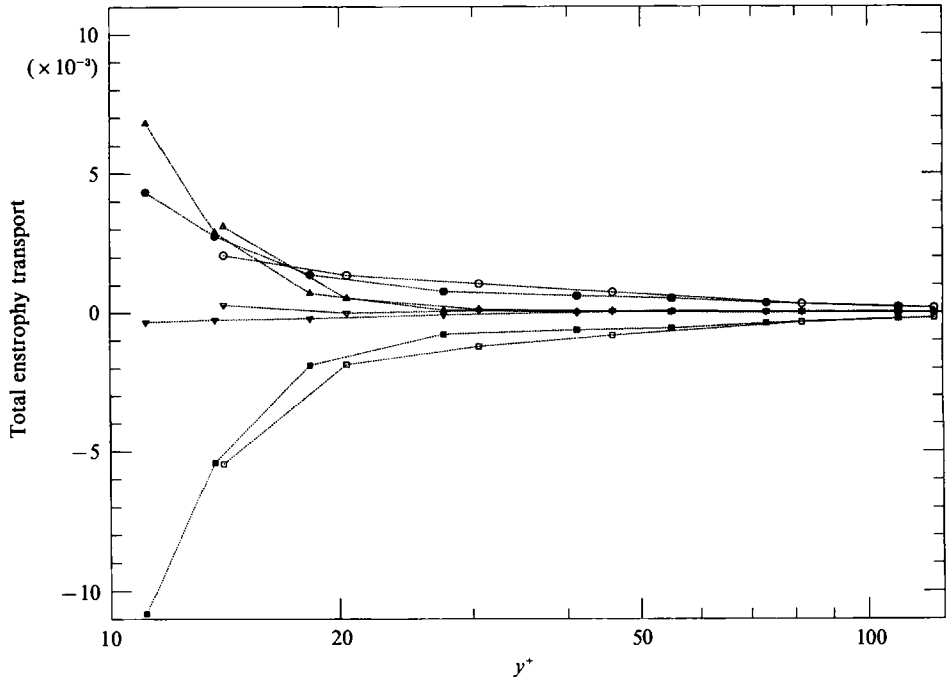

FIGURE 21. Measured terms in equation (7) for the transport of total enstrophy normalized with inner scaling u_τ and ν. Closed symbols, present measurements; open symbols, Balint *et al.* (1990); (▼, ▽), advection (term (7) I); (●, ○), rotation and stretching/compression (term (7) II); (▲, △), viscous diffusion (term (7) III); (■, □), viscous dissipation (term (7) IV).

The terms in (8) and (9) have been interpreted by Tennekes & Lumley (1972) so this will not be repeated here. The advection rate of total enstrophy (term (7) I) is made up of terms (8) I and (8) II in the mean enstrophy equation and terms (9) I, (9) II and (9) III in the fluctuating enstrophy equation. The rotation and stretching/compression rate of total enstrophy (term (7) II) is made up of terms (8) III and (8) IV and (9) IV, (9) V and (9) VI. Terms (8) V and (9) VII combine to form the viscous diffusion rate of total enstrophy (term (7) III). Finally, terms (8) VI and (9) VIII make up the viscous dissipation rate of total enstrophy (term (7) IV). Results for the total enstrophy are shown in figure 21. It appears that the rate of viscous dissipation of total enstrophy is balanced primarily by the viscous diffusion rate close to the wall; however, for $y^+ > 40$ only the rotation and stretching/compression and viscous dissipation rate terms play a significant role. The viscous dissipation rate of total enstrophy cannot be measured with the nine-sensor probe and so must be determined by difference. Thus, these values contain the residual error in the measurement of the other three terms. The mean vorticity and mean vorticity gradients used in determining terms (7) I, (7) II and (7) III were obtained from differentiating a fit of the mean velocity profile. Gradients of vorticity fluctuation correlations were found from graphical slopes. In spite of the rather large inherent errors in these methods, the trends of these terms are repeatable, as seen by the comparison of our present results with those of Balint *et al.* (1990). A comparison with unpublished values computed from the Kim *et al.* (1987) simulation by P. Moin (1990, private communication) confirmed these relative trends, although he obtained larger magnitudes of the terms.

5. Conclusions

The nine-sensor probe used in this boundary-layer experiment measures all the basic statistics of the velocity field with good accuracy. Near the wall there is some attenuation of the measured values because of spatial resolution. Where statistical properties of the vorticity field were available from either other measurements or from direct numerical simulations, our measured values also compared fairly well with them. This demonstrates that the finite-difference approximation we use to estimate the velocity gradients is adequate for the Reynolds number investigated here. The accuracy requirement for the velocity estimate at each of the three arrays is very high, however, in order to get a sufficiently accurate estimate of the velocity gradients.

The following new results have been obtained:

(i) Probability density distributions of the fluctuating vorticity components are quite negatively skewed for the spanwise component in the near-wall region, indicating that intense spanwise vorticity stretching predominates over vorticity compression there.

(ii) Spectra of the fluctuating vorticity components are provided here for the first time for bounded flows. They show the expected shift of maximum energy to higher wavenumbers compared to the velocity spectra, although that shift is not very pronounced at this Reynolds number.

(iii) The balance of terms in the transport equation for total enstrophy shows that viscous dissipation rate is primarily balanced near the wall by the viscous diffusion rate; further from the wall it is balanced by the rotation and stretching rate.

Having established that this probe can be used to measure simultaneously the velocity and vorticity vectors, we plan to investigate the conditional properties of this data set in order to help clarify the structural characteristics of the boundary layer.

We are grateful to S.-R. Park for helping us plot many of the figures. John Kim, Joe Klewicki, Steve Robinson, Philippe Spalart and Tim Wei helpfully provided us with much of the comparison data.

REFERENCES

BALINT, J.-L., VUKOSLAVČEVIĆ, P. & WALLACE, J. M. 1987 A study of the vortical structure of the turbulent boundary layer. In *Advances in Turbulence* (ed. G. Comte-Bellot & J. Mathieu), pp. 456–464. Springer.

BALINT, J.-L., VUKOSLAVČEVIĆ, P. & WALLACE, J. M. 1990 The transport of enstrophy in a turbulent boundary layer. In *Near Wall Turbulence* (ed. S. J. Kline & N. Afgan), pp. 932–950. Hemisphere.

COLES, D. E. 1962 The turbulent boundary layer in compressible fluid. Appendix A: A manual of experimental practice for low speed flow. *Rand Rep.* R403R-PR, ARC24473.

CORRSIN, S. 1953 Interpretation of viscous terms in the turbulent energy equation. *J. Aeronaut. Sci.* **12**, 853–854.

FOSS, J. F. 1981 Advanced techniques for transverse vorticity measurements. In *Proc. 7th Biennial Symp. on Turbulence, University of Missouri-Rolla*, pp. 208–218.

GRESKO, L. S. 1988 Characteristics of wall pressure and near-wall velocity in a flat plate turbulent boundary layer. S.M. Thesis, MIT.

KARLSSON, R. I. & JOHANSSON, T. G. 1988 LDV measurements of higher order moments of velocity fluctuation in a turbulent boundary layer. In *Laser Anemometry in Fluid Mechanics*. Ladoan-Instituto Superior Technico, Lisbon, Portugal.

KASTRINAKIS, E. G. & ECKELMANN, H. 1983 Measurement of streamwise vorticity fluctuations in a turbulent channel flow. *J. Fluid Mech.* **137**, 165–186.

KIM, J., MOIN, P. & MOSER, R. 1987 Turbulence statistics in fully developed channel flow at low Reynolds numbers. *J. Fluid Mech.* **177**, 133–166.

KLEBANOFF, P. S. 1954 Characteristics of turbulence in a boundary layer with zero pressure gradient. *NACA TN*3178.

KLEWICKI, J. C. 1989 On the interactions between the inner and outer region motions in turbulent boundary layers. Ph.D. Dissertation, Michigan State University.

MANSOUR, N. N., KIM, J. & MOIN, P. 1988 Reynolds-stress and dissipation rate budgets in a turbulent channel flow. *J. Fluid Mech.* **194**, 15–44.

PIOMELLI, U., BALINT, J.-L. & WALLACE J. M. 1989 On the validity of Taylor's hypothesis for wall-bounded turbulent flows. *Phys. Fluids* A **1**, 609–611.

PURTELL, L. P., KLEBANOFF, P. S. & BUCKLEY, F. T. 1981 Turbulent boundary layer at low Reynolds numbers. *Phys. Fluids* **24**, 802–811.

SPALART, P. R. 1988 Direct simulation of a turbulent boundary layer up to $R_\theta = 1410$. *J. Fluid Mech.* **187**, 61–98.

SPALDING, D. B. 1961 A single formula for the law of the wall. *Trans. ASME* C: *J. Appl. Mech.* **28**, 455–458.

TENNEKES, H. & LUMLEY, J. L. 1972 *A First Course in Turbulence.* MIT Press.

VUKOSLAVČEVIĆ, P. & WALLACE, J. M. 1981 Influence of velocity gradients on measurements of velocity and streamwise vorticity with hot-wire X-array probes. *Rev. Sci. Instrum.* **52**, 869–879.

VUKOSLAVČEVIĆ, P., WALLACE, J. M. & BALINT, J.-L. 1991 The velocity and vorticity vector fields of a turbulent boundary layer. Part 1. Simultaneous measurement by hot-wire anemometry. *J. Fluid Mech.* **228**, 25–51.

WEI, T. 1987 Reynolds number effects on the small scale structure of a turbulent channel flow. Ph.D. Dissertation, The University of Michigan.

WEI, T. & WILLMARTH, W. W. 1989 Reynolds-number effects on the structure of a turbulent channel flow. *J. Fluid Mech.* **204**, 57–95.